Catalysis Today 182 (2012) 67–79

Contents lists available at ScienceDirect

Catalysis Today

journal homepage: www.elsevier.com/locate/cattod

Structure–activity relationships of simple molecules adsorbed on CPO-27-Ni metal–organic framework: In situ experiments vs. theory

L. Valenzano[a,b], J.G. Vitillo[a], S. Chavan[a], B. Civalleri[a], F. Bonino[a], S. Bordiga[a], C. Lamberti[a,*]

[a] Department of Inorganic, Physical and Materials Chemistry NIS Centre of Excellence, and INSTM reference center, University of Turin, Via P. Giuria 7, I-10125 Torino, 4 Italy
[b] Department of Physics, Michigan Technological University, 1400 Townsend Dr, Houghton, MI 49931-1295, USA

ARTICLE INFO

Article history:
Received 16 June 2011
Received in revised form 13 July 2011
Accepted 17 July 2011
Available online 4 September 2011

Keywords:
MOF
Molecular adsorption
DFT-D* calculation
EXAFS
Powder XRD
FTIR

ABSTRACT

In this work we review experimental XRPD, EXAFS, Raman, IR, microcalorimetric data on the adsorption of H_2O, NO, CO, CO_2, N_2, C_2H_4 and H_2 molecules on CPO-27-Ni material, a metal–organic framework (MOF) showing a coordination vacancy at the Ni^{2+} site in its desolvated form. Literature data are complemented by few new experimental results. A systematic theoretical study performed at the B3LYP-D*/TZVP level of theory (using a periodic boundary conditions) allowed us to reach a complete understanding of the structural, vibrational and energetic features of the material in interaction with the different molecules obtained from the different experimental techniques. From both experimental and theoretical set of data, interesting trends have been obtained for the framework distances (Ni–O and Ni–Ni) and frequency shifts of the framework vibration modes as a function of the adsorption energy (enthalpy) of the different probe molecules. This multitechnical approach, already applied for UiO-66 MOF is of general validity and can be straightforwardly extended to all MOF materials.

1. Introduction

The possibility of tuning framework porosity, topology as well as framework compositions have made zeolites and zeotypes the most successful materials for a broad range of applications like gas adsorption and separation and catalysis [1–20]. But zeolites role as the leading class of crystalline porous materials is nowadays challenged by a new emerging class of porous materials: Metal Organic Frameworks (MOFs) [20–30].

MOFs diverge from zeolites in important ways [31,32], the most important one being their larger diversity and flexibility in composition and less topological constraints in the formation of the porous lattices. The enormous number of new MOF frameworks reported every year reflects this flexibility and the large interest for their potential applications [33]. Zeolites are restricted to tetrahedral networks, the inorganic cornerstone in MOF topologies may be a single metal atom or simple or complex cluster of coordinated metal atoms or extended inorganic sub structures extending in one, two or three dimensions. According to the recent classification done by Tranchemontagne et al. [34] the coordination of the inorganic cornerstone may span the whole range from 3 up to 66. On top of this, cornerstones can be connected using different type of organic linker, giving rise to the synthesis of isoreticular frameworks such as the IRMOF-1/IRMOF-16 [35] or the UiO-66/UiO-68 [36] series.

Although the industrial application of MOFs is still limited to few cases [37,38], this new class of materials is foreseen to play an important role in the next future, in the fields of gas separation and purification [39–48], liquid phase separation [49–52], gas storage [35,53–69], drug delivery [70,71], optical materials [72–76], magnetic materials [77–79], solid state ion conductors [80] semiconductors [81], sensors [82,83], catalysis [82,84–117] and photocatalysis [118].

To foreseen and understand the potentialities of a given MOF structure for both catalytic and gas separation and adsorption applications, the key step is the study of the molecular adsorption at the metal site. This contribution reports part of the examples discussed by Lamberti in the key-note presentation at the 241st ACS Meeting Symposium on "Spectroscopic Techniques to Elucidate Reaction Mechanism and Structure–activity Relationships" held in Anaheim, (CA) March 27–31, 2011. Among all the examples discussed in the symposium, in the present paper, we focus on the CPO-27-Ni case (a Ni^{2+}-MOF exhibiting a coordination vacancy in its desolvated form) because it has been studied in interaction with the largest variety of molecules. This new material, synthesized in Norway by Dietzel et al. [119] belongs to the family of isostructural CPO-27-M (M = Mg, Mn, Fe, Co, Ni, Zn) [64,120–125]. This material is also cited in the literature as MOF-74 or M_2(dhtp).

In this work we review experimental XRPD, EXAFS, Raman, IR, microcalorimetric data recently published [59,119,126–128],

* Corresponding author. Tel.: +39 011 6707841; fax: +39 011 6707855.
E-mail address: carlo.lamberti@unito.it (C. Lamberti).

0920-5861/$ – see front matter © 2011 Elsevier B.V. All rights reserved.
doi:10.1016/j.cattod.2011.07.020

complemented by few new experimental data. Experimental data will be interpreted and rationalized on the basis of unpublished theoretical calculations performed at the B3LYP-D*/TZVP level of theory using a periodic approach (CRYSTAL09 code [129,130]). Using this multi technical approach, a complete understanding of the structural, vibrational and energetic features of CPO-27-Ni after adsorption of H_2O, NO, CO, CO_2 and N_2 is obtained. Partial vibrational and/or energetic information in the adsorption of C_2H_4 and H_2 will also be supplied. This multi technical method, already applied for UiO-66 MOF [131] and here proposed for CPO-27-Ni, is of general validity and can be straightforwardly extended to all MOF materials.

2. Experiments and methods

2.1. CPO-27-Ni synthesis

The CPO-27-Ni material was prepared from a nickel(II) acetate and 2,5-dihydroxyterephthalic acid reaction in a THF–water mixture giving an ochre substance, $Ni_2(dhtp)(H_2O)_2{\cdot}8H_2O$, following a recipe reported in the literature [119]. X-ray powder data showed the high crystallinity of the sample for which a BET surface area of 1200 $m^2\,g^{-1}$ was evaluated (Langmuir surface area of 1315 $m^2\,g^{-1}$). The sample was not sensible to moisture and aging, maintaining its high crystallinity and porosity. To induce dehydration, CPO-27-Ni samples were degassed under high vacuum at 393 K for 1 h. All the spectroscopic and XRPD measurements were performed in controlled atmosphere by using ad hoc cells that allow thermal treatment in high vacuo, dosages of the desired probe molecule and in situ spectra collection to be done. Concerning NO, the gas was carefully purified by distillation in order to remove other undesired nitrogen oxides and it was dosed, by means of a vacuum line, on the samples at RT.

2.2. Experimental methods

FTIR spectra were collected in transmission mode on self-supporting wafer or on a thin film on a silicon wafer, in controlled atmosphere. The spectra were recorded at 2 cm^{-1} resolution on a Bruker IFS 66 FTIR spectrometer, equipped with a liquid nitrogen cooled mercury–cadmium–telluride (MCT) detector. IR spectra reporting the low frequency framework vibrations have been collected using a DTGS detector. Raman spectra were recorded by using a Renishaw Raman Microscope spectrometer. An Ar^+ laser emitting at 514 nm was used, in which the output power was limited to 1% (100% power = 8.2 mW at the sample) in order to avoid sample damage. The photons scattered by the sample were dispersed by a 1800 lines/mm grating monochromator and simultaneously collected on a CCD camera; the collection optic was set at 20× objective. The spectra were obtained by collecting 10 acquisitions (each of 10 s) on a self-supporting wafer put in a home-made cell with a suprasil quartz cuvette that allowed measurements in controlled atmosphere.

Volumetric and calorimetric isotherms of CO and NO adsorption at 303 K were carried out in a microcalorimeter (Tian-Calvet type by Setaram, France) equipped with a calibrated glass gas-volumetric apparatus, which enabled to determine simultaneously the adsorbed amounts and the heat evolved at increasing equilibrium pressure for small increments of the adsorptive [132–137]. The absolute pressures were measured by means of a transducer gauge (Barocell, Edwards, 0–100 mbar). Adsorption microcalorimetry can be easily used to determine the adsorption enthalpy ($-\Delta H_{ads}$) only in cases where the adsorbed molecule reaches a sufficient coverage at room temperature. In the case of N_2 and H_2 molecules, $-\Delta H_{ads}$ has been obtained following the variable temperature IR (VTIR) method, as described elsewhere [128,137–141].

X-ray absorption experiments on Ni K-edge were performed at the BM29 [142] beamline at the European Synchrotron Radiation Facility (ESRF). The monochromator was equipped with two Si(1 1 1) flat crystals and harmonic rejection was achieved using Rh-coated mirrors after monochromator. The following experimental geometry was adopted: (1) I_0 (10% efficiency); (2) MOF sample; (3) I_1 (50% efficiency); (4) reference Ni foil; (5) I_2 (80% efficiency). This set-up allows a direct energy/angle calibration for each spectrum avoiding any problem related to little energy shifts due to small thermal instability of the monochromator crystals [143]. EXAFS spectra were acquired with a sampling step of 0.025 $Å^{-1}$ up to $k = 20\,Å^{-1}$, with an integration time of 3 s/point. Samples, in form of self supported pellets of optimized thickness, have been located inside an ad hoc conceived cell developed at ESRF (by Prestipino, Steinman and Pasternack) that allows evacuation, gas dosage and temperature control in the 77–923 K interval. This experimental set-up guarantees the same degrees of freedom that described in Ref. [144].

The extraction of the $\chi(k)$ function has been performed using Klementev's programs [145]. For each sample, 4 consecutive EXAFS spectra have been collected and corresponding $\chi(k)$ functions have been averaged before data analysis. EXAFS data analysis has been performed using the Arthemis software [146]. Phase and amplitudes have been calculated by FEFF6 code [147] using as input the structure of the hydrated and dehydrated forms of CPO-27-Ni solved by powder X-ray diffraction [119]. For CPO-27-Ni in interaction with CO, NO and N_2, the strategy adopted for the EXAFS refinement has been described in detail elsewhere [126–128] Phase and amplitudes have been successfully checked with NiO model compound [148,149]. For each sample, the averaged $k^3\ \chi(k)$ function were Fourier Transformed in the $\Delta k = 2.00$–$18.00\,Å^{-1}$ interval. The fits were performed in R-space in the $\Delta R = 1.00$–5.00 Å range ($2\Delta k\Delta R/\pi > 40$).

High-resolution X-ray powder diffraction data of the CPO-27-Ni–CO_2 were recorded at the Swiss-Norwegian Beamlines (SNBL/BM01B) at the ESRF using a two-circle diffractometer equipped with 6 counting chains and a wavelength of 0.520054 Å [59]. The sample was hosted inside a 1 mm capillary sealed in CO_2 atmosphere and measured at 100 K.

2.3. Computational methods

Theoretical investigation was carried out using periodic density functional theory (DFT) calculations employing the hybrid B3LYP [150–152] functional empirically corrected to include a long-range dispersion term, as proposed by Grimme [153] and modified for crystalline systems [154]. All calculations were performed with the CRYSTAL09 code [129,130].

All-electron Gaussian-type basis sets were used for all of the atoms. A TZVP basis set was chosen for Ni (Gaussian basis functions' exponents lower than 0.1 au were removed) while a TZP basis set was employed for the adsorbed molecules (vide infra Table 3 for details).

For the numerical integration of the exchange–correlation term a (75,974) pruned grid, was adopted [130]. The condition for the SCF convergence was set to 10^{-8} and 10^{-10} Hartrees during geometry optimization and vibration frequencies calculation, respectively. The Pack-Monkhorst/Gilat shrinking factors for the reciprocal space sampling were set to 2, corresponding to 4 k-points at which the Hamiltonian matrix was diagonalized. The tolerances for one- and two-electron integrals calculation was set to 7 7 7 7 18 (see Ref. [130] for details).

A full relaxation of the structures (both lattice parameters and atomic positions) was performed by keeping the symmetry of the

Table 1
Summary of the structural parameters optimized in the Rietveld refinements of the XRPD patterns.

Sample condition	Dehydrated from Ref. [119]	+H_2O from Ref. [119]	+CO_2 from Ref. [59] [a]
T (K)	295	295	100
$a = b$ (Å)	25.786 ± 0.001	25.9783 ± 0.0007	25.784 ± 0.001
c (Å)	6.770 ± 0.001	6.6883 ± 0.0002	6.7474 ± 0.0003
V (Å^3)	3898.3 ± 0.7	3909.0 ± 0.2	3884.7 ± 0.3
$\langle R_O \rangle$ (Å)	2.00 ± 0.03	2.04 ± 0.02	2.01 ± 0.03
R_{Ni1} (Å)	2.904 ± 0.008	2.980 ± 0.003	2.920 ± 0.002
R_{Ni2} (Å)	4.87 ± 0.01	4.878 ± 0.005	4.869 ± 0.003
R_{ads} (Å)	–	2.08 ± 0.02	2.29 ± 0.02
$\theta_{Ni-O-C}/\theta_{O-C-O}$ (°)	–	–	117.3/162.0

[a] A full coverage has not been reached. From the Rietveld refinement of the CO_2 occupancy factor the authors deduced: $0.5 < CO_2/Ni^{2+} < 0.6$.

system; that is, one molecule was placed on each Ni atom of the unit cell (1:1 molecular loading). All the results refer to Ni in high-spin electronic configuration within a ferromagnetic unit cell. For geometry optimization, the default convergence criteria were used [130]. Equilibrium structures were used to compute the binding energies for the adsorbed molecules (H_2O, CO, CO_2, NO, N_2):

$$\Delta = E_{MOF/X} - E_{MOF} - nE_X \quad (1)$$

where $n = 6$ and X indicates the molecule. Basis set superposition error (BSSE) was taken into account by using the counterpoise correction method [155]. Vibration frequencies referred to the Γ point, were calculated on the optimized geometry by means of a mass-weighed Hessian matrix obtained by numerical differentiation of the analytical first derivatives. Further details can be found elsewhere [156].

From the vibrational frequencies the zero-point vibrational energy (ZPE) and the thermal contribution (H_T) to the enthalpy at a given temperature T was calculated as:

$$H_T = E_{trans}(T) + E_{rot}(T) + E_{vib}(T) + RT \quad (2)$$

for the molecule in the gas phase. $E_{trans}(T)$, $E_{rot}(T)$ and $E_{vib}(T)$ are the translational, rotational and vibrational contributions, respectively, whereas RT accounts for the PV term.

For the solid (MOF with and without the adsorbate) the thermal correction is due only to the vibrational contribution, i.e. $H_T = E_{vib}(T)$.

Finally, the enthalpy of interaction was computed as:

$$\Delta H(T) = \Delta E + \Delta ZPE + \Delta H_T \quad (3)$$

The corresponding value of T was taken to be $T = 100$ K and $T = 298$ K.

Additional computational details, concerning the adsorption of CO and CO_2 on CPO-27-M (M = Mg, Ni, Zn), have been reported elsewhere [157].

3. Results and discussion

3.1. Structure modification upon molecular adsorption: XRPD and EXAFS data vs. theoretical calculations.

3.1.1. Framework structure and XRPD studies

CPO-27 framework contains one-dimensional channels (see Fig. 1d) which are filled with water that can be removed by a mild thermal treatment. Upon dehydration the crystalline structure is preserved and a material with a high surface area containing unsaturated metal sites organized in helicoidal chains (Fig. 1b) is obtained [119]. The chains are connected by the organic ligand with three adjacent chains which results in the honeycomb motif. The channels in the honeycomb have a diameter of ~11 Å and they are filled with solvent. At the intersections of the honeycomb are helical chains of cis-edge connected nickel oxygen octahedra running along the c axis. Nearest neighbors helices are of opposite handedness. All of the O atoms of the ligand (Fig. 1c) are involved in the coordination of Ni^{2+}. These account for five of the oxygen atoms coordinating each nickel atom (Fig. 1a), while the sixth coordinative bond is to a water molecule which points towards the channel.

The structure of CPO-27-Ni in both its hydrated and dehydrated forms was optimized from XRPD Rietveld refinement by Dietzel et al. [119], which main results are summarized here in Table 1. Coordination of water implies an expansion of the cell in the a–b plane of 0.7% and a contraction of the c axis of 1.2%, being the cell volume almost unchanged. The average first shell distance $\langle R_O \rangle$ expands by 0.04 Å to allow the coordination of a water molecule at 2.08 Å, acting as sixth ligand. The first Ni–Ni distance (R_{Ni1}) significantly increases by 0.074 Å, being the second first Ni–Ni distance (R_{Ni2}) almost unchanged. Adsorption of CO_2 at 100 K was investigated in a successive work [59]. No significant modification of the cell in the a–b plane has been observed, while a very small contraction of the c axis (0.3%) has been measured (Table 1). The CO_2 molecule adsorbs in a bent geometry ($\theta_{Ni-O-C} = 117.3°$) at a Ni–O distance of 2.29 Å.

3.1.2. EXAFS studies

The enormous complexity and variety of MOF frameworks [158] represents an evident challenge in the characterization of MOF materials. Only few structures were resolved from single crystal data, due to the difficulty to grow large MOF crystals. In cases were only powder XRD (XRPD) data are available additional structural information, particularly regarding local coordination within the inorganic cluster, are often mandatory in order to solve the structure. In several important cases EXAFS, taking benefit from its atomic selectivity, was able to provide complementary structural information on the inorganic cluster and the way it binds to the ligand [30,36,126–128,131,159–171].

These hydrated and dehydrated structures refined by XRPD have been successively confirmed in the EXAFS study of Bonino et al. [126], see Table 2 and Fig. 2a and b. The XRPD refined structure was used as input for the EXAFS model, resulting in an excellent agreement between the set of distances optimized with the two different techniques. Due to the complexity of the EXAFS signal, reporting important contribution from several SS and MS paths Bonino et al. [126] cross-checked the validity of their EXAFS model analyzing the data collected on dehydrated CPO-27-Ni at 300 and 77 K (see Table 2). The model was validated as all optimized distances were comparable in the two datasets, while the thermal parameters increased moving from 77 to 300 K. The effect of water coordination on CPO-27-Ni significantly affects the EXAFS signal. In particular, $\langle R_O \rangle$ expands from 1.99 ± 0.01 Å to 2.03 ± 0.01 Å, while an even more impressive expansion was observed for R_{Ni1}, that moves from 2.892 ± 0.005 Å up to 2.980 ± 0.005 Å, see Table 2. The $\langle R_O \rangle$ elongation of +0.04 ± 0.02 Å found by EXAFS agrees with XRPD results (+0.04 ± 0.04 Å), the same holds for the elongation of the R_{Ni1} distance (+0.088 ± 0.007 Å) that perfectly matches with the value

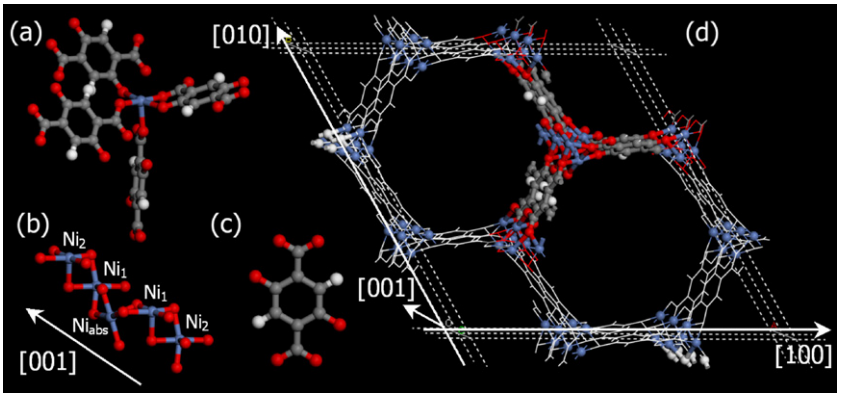

Fig. 1. Pictorial representation, at different magnification grades, of a dehydrated CPO-27-Ni sample. (a) The coordination sphere of Ni^{2+} showing the coordination vacancy. (b) Inorganic nodes involving Ni^{2+} and running along *c* axis. This chain segment contains 5 Ni atoms: supposing that the central one is the X-ray absorber atom (Ni_{abs}) in an EXAFS experiment then, this cluster contains up to the first and second Ni–Ni neighbors, located at R_{Ni1} and R_{Ni2}, both two-fold degenerated. (c) Organic linker. (d) 3D view of the honeycomb structure. The C atoms are reported in grey, H atoms in white, O in red, and Ni in blue. (For interpretation of the references to color in this figure legend, the reader is referred to the web version of the article.)

Table 2
Summary of the parameters optimized by fitting the EXAFS data collected at 77 K. The fits were performed in *R*-space in the 1.0–5.0 Å range over k^3-weighted FT of the $\chi(k)$ functions performed in the 2.0–18.0 $Å^{-1}$ interval. A single ΔE_0 and a single $S_0{}^2$ have been optimized for all SS and MS paths. See Refs. [126–128] for additional fit results ($S_0{}^2$, ΔE, thermal factors, *R*-factors, etc).

Sample condition	Dehydrated from Ref. [126]	Dehydrated from Ref. [126]	+H_2O from Ref. [126]	+NO from Ref. [126]	+CO from Ref. [127]	+N_2 from Ref. [128]
T (K)	300	77	300	300	77	77
$\langle R_O \rangle$ (Å)	1.99 ± 0.01	2.00 ± 0.01	2.03 ± 0.01	2.00 ± 0.01	2.024 ± 0.005	2.012 ± 0.005
R_{Ni1} (Å)	2.892 ± 0.005	2.889 ± 0.005	2.980 ± 0.005	2.94 ± 0.01	2.973 ± 0.005	2.937 ± 0.005
R_{Ni2} (Å)	4.82 ± 0.02	4.87 ± 0.01	4.78 ± 0.03	4.80 ± 0.02	4.89 ± 0.02	4.86 ± 0.02
R_{ads} (Å)	–	–	2.10 ± 0.04	1.87 ± 0.02	2.11 ± 0.02	2.27 ± 0.03
$\theta_{Ni–A–B}$ (°)[a]	–	–	–	130	180	180

[a] The angle $\theta_{Ni–A–B}$ formed between the Ni^{2+} site and the adsorbed molecule has not been optimized but has been assumed in the model used to perform the EXAFS refinement.

obtained from XRPD: $\Delta R_{Ni1} = +0.076 \pm 0.009$ Å. In both dehydrated and hydrated forms, the agreement between EXAFS and XRPD is excellent (within 0.02 Å) for $\langle R_O \rangle$, ΔR_{Ni1} and ΔR_{ads}. The only significant disagreement between EXAFS and XRPD concerns the R_{Ni2} distance of the hydrated system: 0.1 Å. This is probably due to the relative small intensity of the Ni2 atoms signals in the EXAFS spectrum.

The interaction of NO, CO and N_2 ligands with desolvated CPO-27-Ni has been deeply investigated by means of Ni K-edge XANES and EXAFS spectroscopies supported by parallel IR and UV–Vis techniques [126–128] and main results from these studies are summarized here below. EXAFS data (and corresponding best fits) obtained on dehydrated CPO-27-Ni after interaction with NO, CO and N_2 are reported in R-space in Fig. 2c–e and Table 2. The higher intensity of the EXAFS signal in the case of the CPO-27-Ni/CO and CPO-27-Ni/N_2 is evident and is due to the fact that corresponding spectra were collected at 77 K [127,128], while the spectrum of CPO-27-Ni contacted by NO was collected at 300 K [126]. This

Table 3
Summary of the main geometrical and energetic features obtained by periodic calculations at the B3LYP-D*/TZVP level of theory. For comparison also the experimental values for $-\Delta H_{ads}^{expt}$ are reported (n.c. = not computed).

	Dehydrated [this work]	+H_2O [this work]	+NO [this work]	+CO [157]	+N_2 [this work]	+CO_2 [157]
$a = b$ (Å)	26.037	26.114	26.098	26.093	26.103	26.156
c (Å)	6.851	6.914	6.858	6.928	6.907	6.863
V ($Å^3$)	4022.3	4083.1	4045.0	4084.9	4075.5	4066.2
$\langle R_O \rangle$ (Å)	2.034	2.069	2.057	2.066	2.053	2.049
R_{Ni1} (Å)	2.936	3.015	2.997	3.029	2.990	2.968
R_{Ni2} (Å)	4.926	5.002	4.966	5.017	4.984	4.950
R_{ads} (Å)	–	2.153	2.101	2.148	2.281	2.337
$\Delta d_{AB}/\Delta d_{BC}$ (Å)[a]	–/–	+0.005/+0.006	−0.008/–	−0.005/–	−0.002/–	+0.006/−0.007
$\theta_{Ni–A–B}$ (°)	–	100.0/110.1	123.2	171.8	170.9	124.0
$-\Delta E^c$ (BSSE) (kJ mol^{-1})	–	74.7 (11.2)	49.1 (14.0)	46.2 (7.7)	27.3 (8.5)	38.9 (6.1)
ΔZPE (kJ mol^{-1})	–	n.c.	n.c.	4.5	n.c.	2.0
$-\Delta H_T$ (100 K)/$-\Delta H_T$ (298 K) (kJ mol^{-1})	–	n.c.	n.c.	1.4/0.2	n.c.	0.6/+1.4
$-\Delta H^0$ (100 K)/$-\Delta H^0$ (298 K) (kJ mol^{-1})	–	n.c.	n.c.	43.1/41.9	n.c.	37.6/35.5
$-\Delta H_{ads}^{expt}$ (kJ mol^{-1})[b]	–	>100	92	58	17	38

[a] Intra-molecular distances of the adsorbed $Ni^{2+}\cdots AB(C)$ molecule: AB(C) = OH_2; NO; CO; NN; O–C–O. For the unperturbed molecules the distances computed at B3LYP-D*/TZVP level of theory are: $d_{AB} = d_{BC} = 0.963$ (OH_2); $d_{AB} = 1.148$ (NO); $d_{AB} = 1.127$ (CO); $d_{AB} = 1.093$ (N_2); $d_{AB} = d_{BC} = 1.161$ (CO_2). All values in Å. The intra molecular angle $\theta_{O–C–O}$ for the adsorbed CO_2 molecule has been optimized at 178.2°.

[b] $-\Delta H_{ads}^{expt}$ values are obtained by microcalorimetry for NO and CO (Refs. [126,127], respectively), by VTIR for N_2 (Ref. [128]) and by isosteric heat for CO_2 (Ref. [124]). The experimental adsorption enthalpy for water has been proved to be higher than that of NO, being able to displace it at room temperature [126].

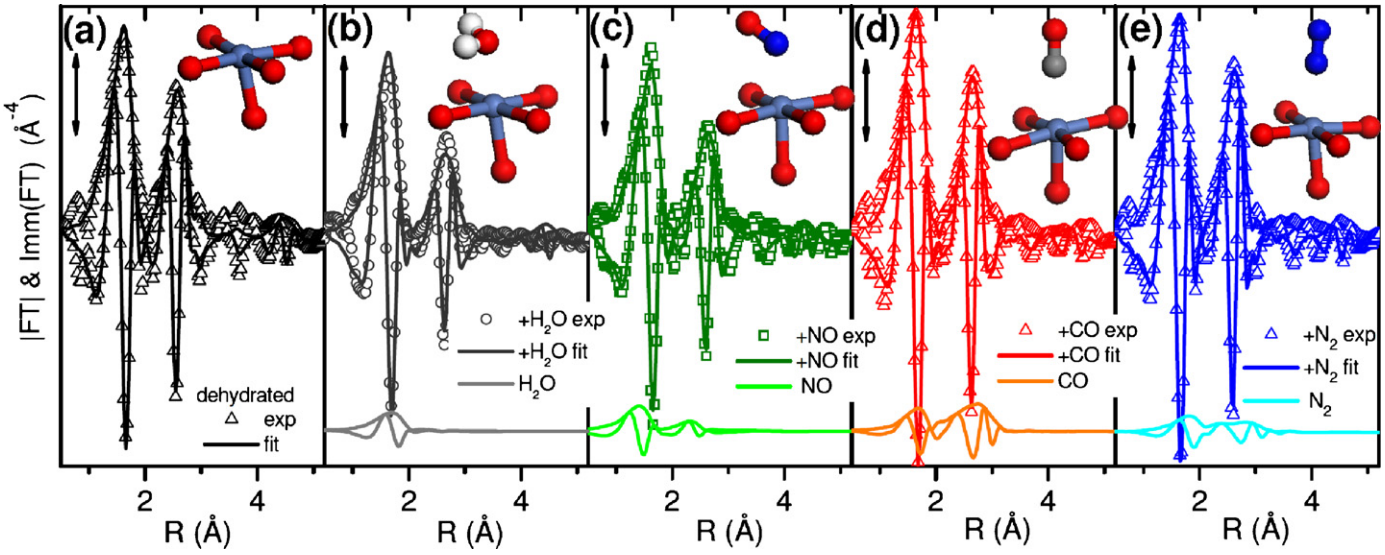

Fig. 2. Modulus and imaginary part of the k^3-weighted, phase uncorrected, FT of the EXAFS spectra collected on dehydrated CPO-27-Ni (a) and after interaction with H_2O and NO at 300 K and CO and N_2 at 77 K, (b)–(e), respectively. 300 and 77 K experimental data are reported as scattered circles and triangles, respectively, while the corresponding best fits are reported as continuous lines. Where adsorbates are present, vertically translated also the contribution (in both modulus and imaginary parts) of the adsorbed molecule optimized in the fits is reported. The models used in the fits adopted a Ni^{2+}/adsorbate = 1:1 stoichiometry and assumed a linear adsorption geometry for CO and N_2 and a Ni–N–O angle of 130° for the NO (only the O atom of the H_2O molecule has been included in the fit). Insets report the local environment of Ni^{2+} in its dehydrated form, part (a), and upon molecular adsorption parts (b)–(e).

Unpublished figure: the EXAFS spectra have been adapted from Refs. [126–128].

implied that authors were forced to fix much more parameter in the analysis of the case of NO adsorption. Independent IR and volumetric-calorimetric experiments allowed to fix the coordination number of the adsorbed molecules (NO, CO and N_2) to 1 [126–128].

In the bottom of Fig. 2(b)–(e) we report the contribution of the adsorbed molecule to the overall fit. For the water molecule (Fig. 2(b)), only a single Ni–O contribution is visible, being negligible the scattering from the H atoms. For the diatomic molecules both first and second atom contributions are visible. For CO and N_2 (Fig. 2d and e), both signals are of comparable intensity because the contribution of the MS paths, contributing at the same distance as the second atom, and are enhanced by paths co-linearity [172–177]. Due to the bent nature of the adduct, this enhancement is quenched for the NO case, leading to a higher distance contribution which is much weaker than that coming from shorter distance (see Fig. 2c). The difficulties of the EXAFS analysis of these spectra is related to the combined facts that (i) the contribution of the adsorbed molecules lies in the same R region where the strong Ni–O and Ni–Ni contribution of the framework appears (ii) the contribution of the framework is significantly modified by molecular adsorption. On the basis of our EXAFS study the following scale in the ability to perturb the framework can be defined: N_2 at 77 K ≤ NO at 300 K < CO at 77 K ≤ H_2O at 300 K.

The Ni–N distance of the $Ni^{2+}\cdots$NO adduct was optimized at 1.85 ± 0.02 Å. NO adsorption causes an almost negligible modification of the average Ni–O first shell distance that does not undergo the stretching observed when water was coordinated (see Table 2), while the R_{Ni1} distance increases by +0.051 ± 0.011 Å. In their original paper Bonino et al. [126] refined the EXAFS spectrum using both a linear and a bent $Ni^{2+}\cdots$NO adduct as model, obtaining similar results. Here, supported by the DFT calculation (vide infra Table 3) we report the results obtained with the bent model only.

Concerning the interaction with CO, the fit of the EXAFS spectrum (see Fig. 2d and Table 2) results into a Ni–CO distance of 2.11 ± 0.02 Å. As expected, all distances undergo an elongation with respect to the dehydrated case: $\langle R_O \rangle$ moves from 2.00 ± 0.01 Å to 2.024 ± 0.005 Å, R_{Ni1} from 2.889 ± 0.005 Å to 2.973 ± 0.005 Å, and R_{Ni2} from 4.87 ± 0.01 Å to 4.89 ± 0.02 Å. The small elongation of the first shell distance (+0.024 ± 0.011 Å) is typical of an adsorption process that saturates one or more coordinative vacancies. Conversely, the much more relevant increase of the second shell distance (+0.084 ± 0.007 Å) is peculiar of this MOF structure, and has already been observed with other adsorbates, like H_2O (+0.088 ± 0.007 Å from RT EXAFS data [126], and +0.076 Å from XRPD [119]) or NO (+0.051 ± 0.011 Å from RT EXAFS data) [126]. As already done for the dehydrated material [126], the validity of the model was checked on the EXAFS spectrum collected at RT in presence of CO.

The EXAFS spectrum of the CPO-27-Ni/N_2 system has been analyzed using the same approach applied for the CPO-27-Ni/CO system, thus assuming a linear Ni–N–N adsorption geometry (R_{N-N} = 1.10 Å) [128]. The quality of the fit can be appreciated in Fig. 2e. N_2 adsorption causes a small elongation of the first shell Ni–O bond length ($\langle R_O \rangle$), averaged over five contributions, from 2.00 ± 0.01 Å to 2.012 ± 0.005 Å and a larger elongation of the first Ni–Ni distance (R_{Ni1}) from 2.889 ± 0.005 Å to 2.937 ± 0.005 Å. Such modifications are similar, even if less important, to those observed upon NO or CO adsorption, see Table 2.

3.1.3. Theoretical study

The main geometrical and energetic results obtained by periodic calculations at the B3LYP-D*/TZVP level of theory with the CRYSTAL09 code [129,130] are summarized in Table 3, while the optimized structures are reported in Fig. 3, viewed along the [001] direction. All the results refers to CPO-27-Ni and to a molecular loading 1:1 (one molecule per metal atom) with nickel atoms in high-spin electronic configuration within a ferromagnetic unit cell.

The structure of CPO-27-Ni in absence of adsorbates is perfectly reproduced by calculations, being the error in the determination of the *a* and *b* lattice cell parameters within 1% (3% for the cell volume). The agreement for $\langle R_O \rangle$ and R_{Ni1} distances is as good as 0.03 Å when comparison is made with the XRPD data and within 0.01 Å with EXAFS. A value that increases up to 0.05 Å for the R_{Ni2} distance. In all cases the computed vales overestimate the experimental ones.

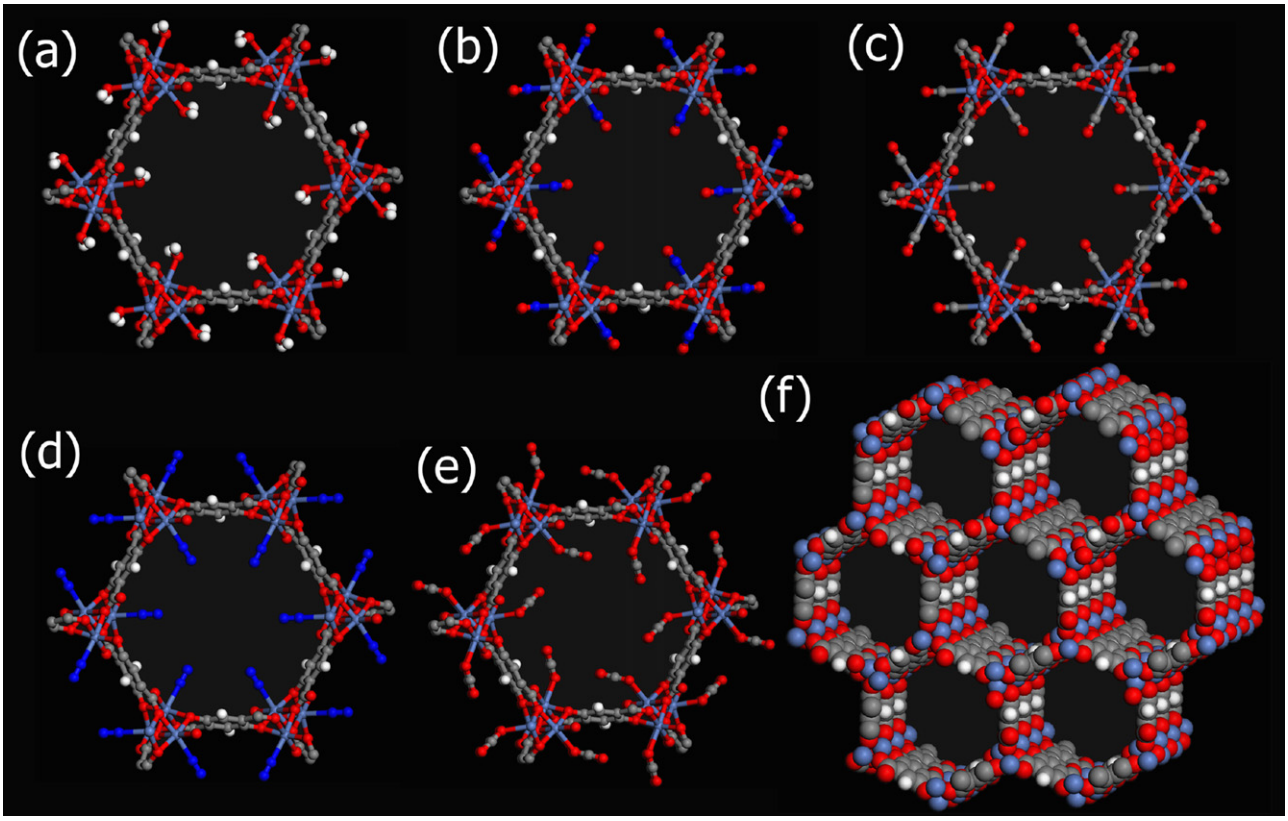

Fig. 3. Optimized periodic structures at B3LYP-D*/TZVP level of theory. (a) CPO-27-Ni + H_2O; (b) CPO-27-Ni + NO; (c) CPO-27-Ni + CO; (d) CPO-27-Ni + N_2; (e) CPO-27-Ni + CO_2; (f) dehydrated CPO-27-Ni. In (a)–(e) cases a 1:1 Ni^{2+}: molecules coverage has been adopted. (a)–(e) Viewed from the [0 0 1] direction, while a slightly tilted view has been chosen for part (f) to allow to appreciate the 3D structure. Unpublished.

As expected, adsorption of all investigated molecules causes an expansion of the unit cell volume that is due to an increase of both *a* and *c* lattice parameters. ΔV is larger for CO and H_2O (1.5%) because of a lengthening of Ni–O bonds along the *c* lattice constant. This is also evident in the elongation of the Ni–Ni distances, that in the case of CO are: ΔR_{Ni1} = +0.093 Å and ΔR_{Ni2} = +0.091 Å. These values have to be compared with those obtained from EXAFS: ΔR_{Ni1} = +0.084 ± 0.007 Å; ΔR_{Ni2} = +0.02 ± 0.03 Å. The optimized adsorption angle, θ_{N-C-O} = 171.8°, well support the linear model used to refine the EXAFS spectrum. An excellent agreement is also found for the R_{ads} distance, computed at 2.148 Å, while EXAFS locate the CO molecule at R_{ads} = 2.11 ± 0.02 Å. Surprisingly, the optimized $Ni^{2+}\cdots$CO distance (2.148 Å) is very close to the computed distance for CO adsorbed on the homologue CPO-27-Mg material (R_{ads} = 2.486 Å, see Ref. [125]): note that for the $Mg^{2+}\cdots$CO adduct no σ nor π charge transfer effects are expected. As the IR spectra reported by Chavan et al. [127] indicate that $Ni^{2+}\cdots$CO interaction show a small π-back-donation contribution, a shorter adsorption would be expected for the nickel case. A possible explanation is that the small π-back-donation contribution in CPO-27-Ni is partly compensated by the deformation of structure, so that CO distance turns out to be similar to that of the $Mg^{2+}\cdots$CO adduct. Note that the CO distance depends on a delicate balance between electrostatics and charge-transfer effects.

For NO, a similar behavior is observed as for CO because of a marked influence of charge transfer effects. Therefore, longer $\langle R_O \rangle$, R_{Ni1} and R_{Ni2} distances are predicted. Conversely, the unit cell volume is the smallest among the computed ones because of the small size of the NO molecule and of the structure of the $Ni^{2+}\cdots$NO complex that forms an angle of θ_{Ni-N-O} = 123.2°. A similar arrangement was also observed for NO in interaction with Ni^{2+} sites in analogous systems. Freund et al. [178] found for the NO/NiO(0 0 1) system a value θ_{Ni-N-O} = 135° according to the evolution in the Ni K-edge NEXAFS spectra as a function of the angle between the polarization axis of the exciting photons and the NiO surface of the ratio between the peaks due to the $1s \rightarrow \sigma$ and $1s \rightarrow 2\pi$ resonances. This experimental evolution was fitted with theoretical curves obtained changing the θ_{Ni-N-O} angle in the 90–180 range. Again on the NO/NiO(0 0 1) system Bradshaw et al. [179] found θ_{Ni-N-O} = 120° and R_{ads} = 1.88 ± 0.02 Å by photoelectron diffraction. Pacchioni et al. [180,181] explained the EPR spectra obtained on NO adsorbed on Ni-doped MgO(0 0 1) surfaces using spin restricted RO-B3LYP calculation on cluster model. The optimized geometry was θ_{Ni-N-O} = 119.5° and R_{ads} = 1.789 Å. The optimized for the $Ni^{2+}\cdots$NO adduct in CPO-27-Ni (Table 3) is clearly overestimated with respect to both the experimental value obtained by EXAFS (Table 2) and the experimental and theoretical results obtained on similar systems discussed above.

For CPO-27-Ni with CO_2, the expansion of the unit cell is less pronounced: $\Delta V/V$ = 1.1%. The computed *a* lattice constant is the largest among studied systems ($\Delta a/a$ = 0.5%, see Table 3), but the *c*-axis expands only by 0.012 Å. Experimental lattice parameters (Table 1) behave differently upon CO_2 adsorption being *a* almost unaffected, while *c* is slightly contracted. Computational results are explained on the basis of the angular geometry of the $Ni^{2+}\cdots$OCO complex as a result of a lateral interaction between the CO_2 molecule and the O atom of the nearby carboxylate group due to the electrostatic interaction with the quadrupole moment of CO_2 (Fig. 3e). It is worthy to note that this secondary interaction with the organic linker agrees with experimental XRPD measurements [182].

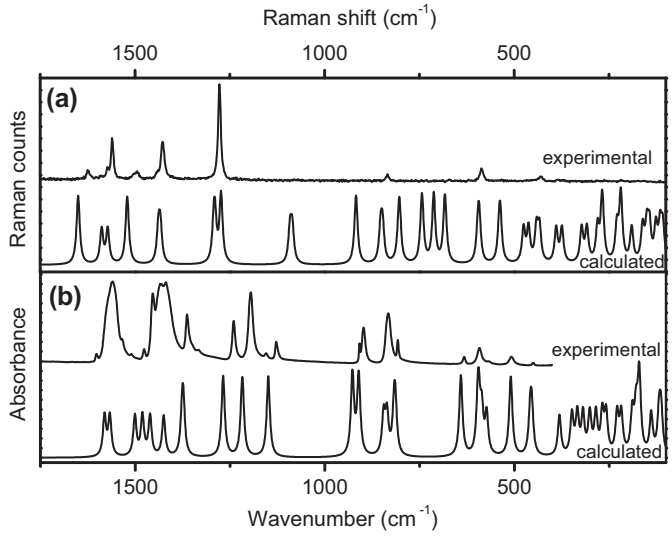

Fig. 4. Comparison between experimental (top) and calculated (bottom) vibrational features of the dehydrated CPO-27-Ni material. (a) Raman spectra. (b) IR spectra. No scaling factor has been adopted to match computed spectra with the experimental ones. For IR spectra both band frequencies and intensities have been computed, while only the frequency positions have been computed for the Raman modes: the Raman spectrum has been obtained by adding Gaussian curves centred at the computed frequency with the same intensity and a FWHM of 10 cm^{-1}. Consequently, simulated bands appearing as more intense just reflect the presence of more than one Raman active mode within the adopted FWHM. Unpublished.

However, in the experimental structure the molecule is also bent with a O–C–O angle of $\theta_{O-C-O} = 162.0^{\circ}$. This does not appear in the predicted B3LYP-D* structure, where $\theta_{O-C-O} = 178.2^{\circ}$. The observed bent angle (θ_{O-C-O}) seems affected by a large error and there is no evidence from IR spectroscopy of a large shift for the bending

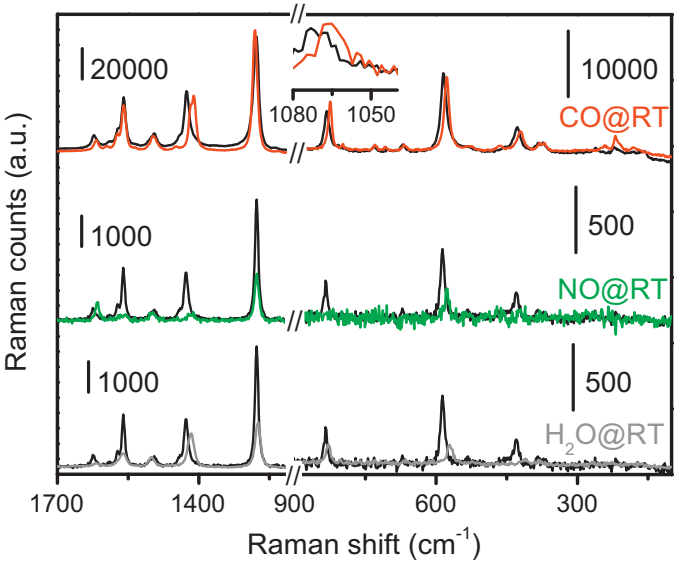

Fig. 5. Modification of the experimental Raman spectra, collected at RT, upon molecular adsorption on Ni^{2+} site, from top to bottom: CO, NO and H_2O. In all cases the spectrum collected on the dehydrated material, is reported in black for comparison. The spectra collected before and after CO dosage (top spectra) have been collected with a five time longer integration time: this explains the significantly higher signal to noise ratio, allowing to detect a weak band at 1072 cm^{-1}, that downward shift at 1065 cm^{-1} upon CO adsorption. In order to allow a direct comparison among the different spectra, the intensity of all bands has been normalized to the intensity of the component around 1500 cm^{-1}, that is the band showing the smaller shift upon molecular adsorption.

Unpublished figure: data adapted from Refs. [126,128].

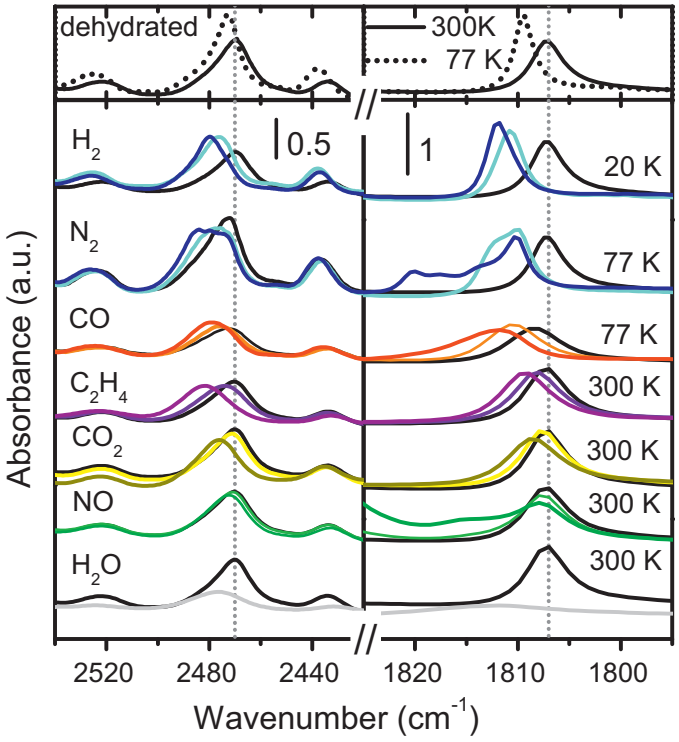

Fig. 6. Top: modification of the experimental IR spectrum of dehydrated CPO-27-Ni as a function of temperature. Bottom: Modification of the experimental IR spectra upon molecular adsorption on Ni^{2+} site at different coverages. In all cases the spectrum collected at 300 K on the same pellet (previously dehydrated) before molecular adsorption is reported in black for comparison. Minor differences of the different background curves reflect differences in both the pellet thickness and the dehydration treatment. For each case, the temperature at which the spectra have been collected is also reported. Unpublished.

mode of CO_2 (vide infra Fig. 7). Overall, the good agreement between computed B3LYP-D* data and both vibration frequency shifts and calorimetric binding energies (see below) would suggest that CO_2 is not bent. Finally, the Ni^{2+}-adsorbate distance is optimized at $R_{ads} = 2.29 \pm 0.02$ Å and 2.337 Å in XRPD and B3LYP-D* methods, respectively. The fact that experimental XRPD pattern has been collected on a sample exhibiting a coverage CO_2/Ni^{2+} coverage of only 0.5, while a full coverage has been used in the periodic calculations, can only partially explain these disagreements.

Interaction of Ni^{2+} with N_2 is less specific and more ruled by electrostatics. Therefore, nitrogen molecule is only slightly perturbed as observed in the small frequency shifts (vide infra Section 3.2). In turns the perturbation induced on the CPO-27-Ni framework by N_2 adsorption are weak too, but they have been appreciated by both B3LYP-D* calculations and EXAFS measurements. Remarkable is the agreement obtained in determination of the adsorption distance: $R_{ads} = 2.281$ Å from calculations and $R_{ads} = 2.27 \pm 0.03$ Å from EXAFS.

3.2. *Vibrational features before and after molecular adsorption: IR, Raman data vs. theoretical calculations.*

A complete understanding of the vibrational features of CPO-27-Ni material has been obtained from the periodic B3LYP-D* calculation performed with CRYSTAL code. Fig. 4 reports a direct comparison between computed and experimental vibrational spectra: both Raman (part a) and IR (part b). Actually the simulated Raman spectrum represents the vibrational DOS, as no intensity calculations have been performed. In both cases the main vibrational features are well reproduced by the calculation. The perturbation of the main vibrational features upon molecular adsorption is

reported in Figs. 5 and 6 for the Raman and IR spectra respectively. In all cases the spectrum collected on the dehydrated material, is reported in black for a direct comparison.

The hydrated form of CPO-27-Ni, black spectrum in Fig. 5, the bands at 1625, 1561 and 586 cm^{-1} are due to benzene ring vibrations, being the two at higher frequency due to stretching modes and the lower one to a ring deformation [126]. Features at 1495 and 1428 cm^{-1} are assigned to $\nu(COO^-)_{asym}$ and $\nu(COO^-)_{sym}$. The intense band at 1277 cm^{-1} is attributed to ν(CO) vibration due to the deprotonated species derived from the hydroxyl group. The minor feature at 835 cm^{-1} is ascribed to ring C–H bending modes [75,126,166]. At lower frequency, the band at 430 cm^{-1} is attributed to the $\nu(Ni–O_{Ligand})$ mode [126,183]. Upon water coordination, some relevant changes occur in the framework vibrational region in both the frequency and the relative intensities of the Raman bands. As far as the frequency shifts are concerned, most of the components are sensibly red-shifted (the bands at 1625, 1561, 1427, 1278, 833, 586 and 430 cm^{-1} move respectively to 1618, 1558, 1415, 1273, 827, 570 and 410 cm^{-1}). Please note that in the original paper these bands were wrongly reported. Exception is made for the band around 1500 cm^{-1}, that remains almost un-shifted, or slightly red-shifted. A global increase in intensity of all the spectrum features can be justified by considering that upon water coordination the framework undergoes an increase of local symmetry.

Adsorption of NO modifies the spectrum red-shifting the bands (as was the case for water) but also significantly altering the relative intensities. Most of the bands decrease in intensity while some almost disappears. In particular, upon NO interaction, (i) the most affected bands are those at 1560 and 1426 cm^{-1}, that lose about 1 order of magnitude in intensity and are slightly red-shifted (at 1555 and 1417 cm^{-1} respectively); (ii) the components at 1275 and 585 cm^{-1} lose almost 50% of their intensity, the former does not shift, whereas the latter shifts at 578 cm^{-1}; (iii) the very week bands at 833 and 430 cm^{-1} fail below the signal to noise ratio. Finally the band at 1625 cm^{-1} makes exception, doubling its intensity, while undergoes a red-shift to 1615 cm^{-1}.

CO adsorption strongly perturbs some framework modes of the CPO-27-Ni, while other are left unchanged. In particular the bands at 1625 and 586 cm^{-1}, assigned to benzene ring vibrations, shift to 1616 and 575 cm^{-1} respectively; the bands at 1427 and 833 cm^{-1}, due to $\nu(COO^-)_{sym}$ and δ(CH), move to 1410 and 824 cm^{-1} and the ν(Ni–O) band at 430 cm^{-1} is shifted at 419 cm^{-1}.

Fig. 6 reports two selected wavenumber intervals containing framework modes particularly affected by molecular adsorption. The amount of the perturbation, measured in terms of band shift is determined by three main factors: (i) the equilibrium pressure; (ii) the adsorption temperature (iii) the adsorption enthalpy. The effect of the equilibrium pressure can be appreciated for all the cases where an intermediate spectrum has been reported, using a paler color code. The effect of temperature is particularly evident in the top part of the figure where the spectra of the dehydrated material collected at 300 and 77 K are reported as full and dotted black lines, respectively. Taking this effect into account, it is evident that the important shift observed upon H_2 adsorption at 20 K is by about 40% due to a thermal effect, being the actual effect of molecular absorption only about 60% of the overall shift. Finally, the effect of adsorption enthalpy can be appreciated in all the set of spectra collected at the same temperature.

So far we discussed how molecular adsorption perturbs the CPO-27-Ni framework modes. As for the perturbation induced by Ni^{2+} and its environment perturb the molecular modes, the following shifts, with respect to the unperturbed molecule, have been experimentally observed for the unique stretching mode of the diatomic molecules: $\Delta\nu$(NO) = −31 cm^{-1} [126]; $\Delta\nu$(CO) = +35 cm^{-1} [127]; $\Delta\nu$(NN) = +11 cm^{-1} [128]; $\Delta\nu$(HH) = −126 cm^{-1} [60]. For C_2H_4 the following shifts were observed: $\Delta\nu_1$ = −19 cm^{-1}; $\Delta\nu_{11}$ = −11 cm^{-1}; $\Delta\nu_7$ = +34 cm^{-1}; [128].

On a computational ground, among discussed molecules the vibrational modes have been calculated for the CO and CO_2 cases only. When the CO molecule is introduced in the CPO-27-Ni framework, different modes of mainly ν(CO) nature appear, depending on how the relative motion of the different CO molecules. Using a full harmonic approach, these modes results in $\Delta\nu$(CO) in the 36–38 cm^{-1} range. If anharmonicity is taken into account, these values slightly shift to 35–41 cm^{-1}. These results are in perfect agreement with the experimental IR spectra that shows a rather broad band centred at $\Delta\nu$(CO) = +35 cm^{-1} [127], see Fig. 7a.

The case of CO_2 is more complex, as the correct reference to compute the frequency shift is not the vibrational mode of the molecule in the gas phase ν_3 = 2349 cm^{-1} but the value obtained for the adsorption in silicalite corrected by the interaction with silanols (ν_3 = 2338 cm^{-1}) [184]. Please note that also in the case of N_2 adsorbed on zeolites, the frequency shift was computed from the Raman mode of N_2 in silicalite [185]. The IR spectra of CO_2 adsorbed at RT on CPO-27-Ni are reported in Fig. 7b in the ν_3 stretching region. Two narrow and distinct bands are observed at 2342 and 2329 cm^{-1}, resulting in $\Delta\nu_3$ = +4 and −9 cm^{-1}, respectively. Computed full harmonic frequency shifts are $\Delta\nu_3$ = +8 and −3 cm^{-1}, again in excellent agreement with the experiment. The calculations allow to associate the mode at 2329 cm^{-1} to a double degenerate E_u mode showing either all the six CO_2 molecules hosted in the cavity (see Fig. 3e) participating in phase to the motion or only four of them vibrating, the remaining two (opposite with respect to the C_6 axis of the channel) acting as spectators. The mode at 2342 cm^{-1} is due to an A_u mode involving all the six molecules oscillating out of phase. Note that the splitting of the ν_3 modes has been clearly observed in the bending region also (Fig. 7c), where two distinct bands are observed at 660 and 652 cm^{-1}, in the high energy side of the IR strong framework mode at 635 cm^{-1}.

3.3. Energetic of molecular adsorption: microcalorimetry and VTIR data vs. theoretical calculations. Rationalization of structural and vibrational perturbations

3.3.1. Summary of experimental results

For both NO (92 kJ mol^{-1}) and CO (58 kJ mol^{-1}) the adsorption enthalpies have been measured at 303 K by microcalorimetry in Refs. [126,127], respectively. Corresponding primary volumetric and calorimetric isotherms are reported here in parts (a) and (b) of Fig. 8 for a direct comparison. NO rapidly reaches a 1:1 adsorption, even at the lowest equilibrium pressures (P_e), while CO reaches high coverages at higher P_e (Fig. 8a). Secondary adsorption isotherms (not reported for clarity) indicates that CO is fully reversible at 303 K, while NO exhibits about 80% of irreversible adsorption. The differential molar adsorption heat q_{diff} reported Fig. 8b show a rather week dependence on the coverage and the corresponding zero coverage limits results in the $-\Delta H_{ads}$ values of 92 and 58 kJ mol^{-1} reported in Table 3 for NO and CO, respectively.

In the case of N_2 and H_2 molecules that do not adsorb at room temperature on Ni^{2+} sites of CPO-27-Ni material, $-\Delta H_{ads}$ has been obtained following the variable temperature IR (VTIR) method [128,137–141]. The procedure consists in the measurement of the intensity of the IR band of the adsorbed molecule as a function of the temperature T. Its intensity increases gradually upon decreasing T till it reaches a maximum (I_{max}), corresponding to saturation conditions. The ratio between the intensity measured at a given T ($I(T)$) and that at saturation conditions (I_{max}) allows to quantitatively know the fraction of Ni^{2+} sites in interaction with the adsorbed molecule molecules defined as $\theta(T) = I(T)/I_{max}$ and, consequently, the fraction $1-\theta(T)$ of unengaged Ni^{2+} sites. In this way, the equilibrium constant (K_{ads}) of the $Ni^{2+}\cdots N_2$ ($Ni^{2+}\cdots H_2$)

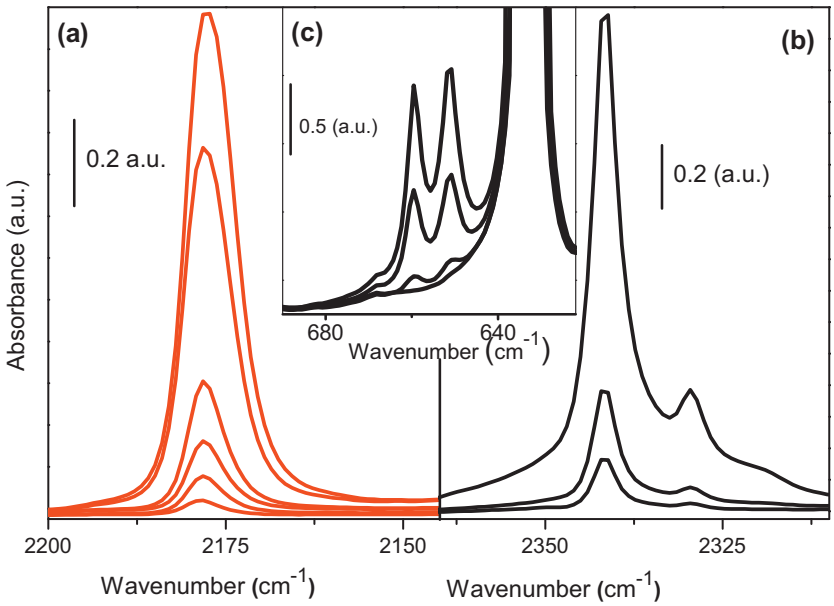

Fig. 7. (a) Background subtracted IR spectra, in the ν(CO) stretching region, of CO dosed on at room temperature on CPO-27-Ni as a function of CO equilibrium pressure. (b) As part (a) for the CO_2 dosage, spectra reported in the ν_3 stretching region. (c) As in part (b), reported in the CO_2 bending region (higher CO_2 equilibrium pressure are reported here, with respect to part (b). (a) and (b) reported using a wavenumber interval of the same amplitude ($\Delta\nu = 55\ cm^{-1}$), so that the FWHM of the bands due to $Ni^{2+}\cdots CO$ and $Ni^{2+}\cdots OCO$ adducts can be directly compared.

Unpublished figure, adapting data from Refs. [59,127].

complex formation at any given temperature can be described, under the Langmuir approximation, as $K_{ads}(T) = \theta(T)/\{[1-\theta(T)]P_e\}$. Applying the van't Hoff equation, the slope of the $\ln(K_{ads})$ vs. $1/T$ gives the enthalpy of $Ni^{2+}\cdots N_2$ ($Ni^{2+}\cdots H_2$) complex formation. The values of $K_{ads}(T)$ obtained from the IR spectra reported have been plotted vs. $1/T$ in Fig. 8c for both molecules. The slope of the best linear fit of the reported data gives the value of $-\Delta H_{ads} = 17$ and 13.5 kJ mol^{-1}, for the $Ni^{2+}\cdots N_2$ and $Ni^{2+}\cdots H_2$ complex formation, respectively. These values are significantly lower than those found for the formation on the same sites for $Ni^{2+}\cdots NO$ and $Ni^{2+}\cdots CO$ complexes, 92 and 59 kJ mol^{-1}, respectively, but they are still important for a complex formed with inert molecules.

The isosteric heat of adsorption for CO_2 has been determined by Dietzel et al. [124] to be 38 kJ mol^{-1}, a value that is in perfect agreement with the independent one reported by Caskey et al. [123]: 41 kJ mol^{-1}.

3.3.2. Description of the theoretical results

As all calculations have been performed at a $\theta = 1$ coverage we have six adsorbed molecules per CPO-27 ring (see Fig. 3), that are spaced by about 6 Å along the c axis to the adjacent set of six adsorbed molecules. In such conditions the lateral interactions among adsorbates are less than 1 kJ mol^{-1}. In particular, they are 0.8, 0.04, 0.6 and 0.8 kJ mol^{-1}, for CPO-27-Ni in interaction with CO and CO_2, NO and N_2, respectively. Computed adsorption energies include the lateral interaction energy.

The large role played by dispersion interactions, in all cases, has been proved by performing the same calculations without

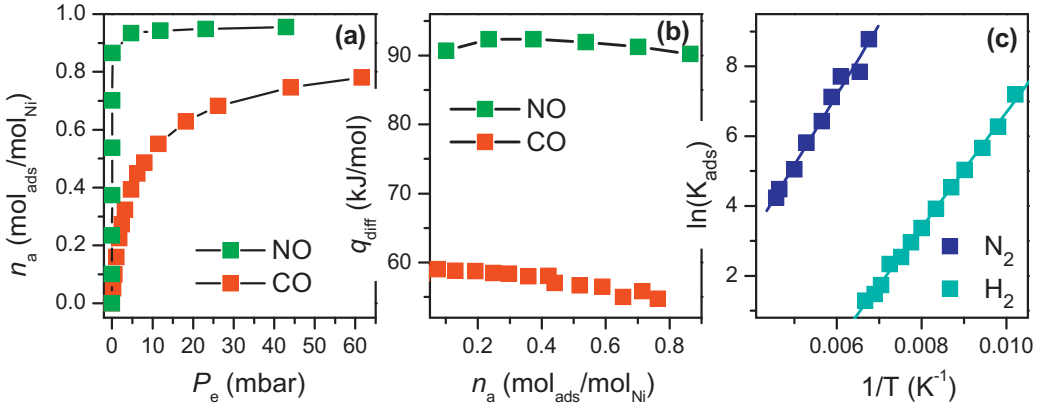

Fig. 8. (a) Plot of the primary excess volumetric isotherms obtained for NO (green squares) and CO (red squares) adsorption on CPO-27-Ni at 303 K as a function of the equilibrium pressure P_e. The molar NO (and CO) amounts n_a have been normalized to the moles of Ni atoms present in the CPO-27-Ni sample, supposing all the Ni atoms available to the interaction with the adsorbed molecule. Secondary excess volumetric isotherms (not reported for brevity) show 80% and 0% of irreversible adsorption at 303 K for NO and CO, respectively. (b) Dependence of the differential molar adsorption heat q_{diff} on the molecular coverage n_a, obtained for NO (green squares) and CO (red squares). (c) Plot of the dependence of ln K (obtained from temperature dependent IR experiments) vs. $1/T$ for the formation of $Ni^{2+}\cdots N_2$ (blue squares) and $Ni^{2+}\cdots H_2$ (cyan squares) adducts in CPO-27-Ni. The slope of the best linear fits gives the $-\Delta H_{ads}$ values for the formation of the two adducts. (For interpretation of the references to color in this figure legend, the reader is referred to the web version of the article.)

Unpublished Figure: data adapted from Refs. [60,126–128].

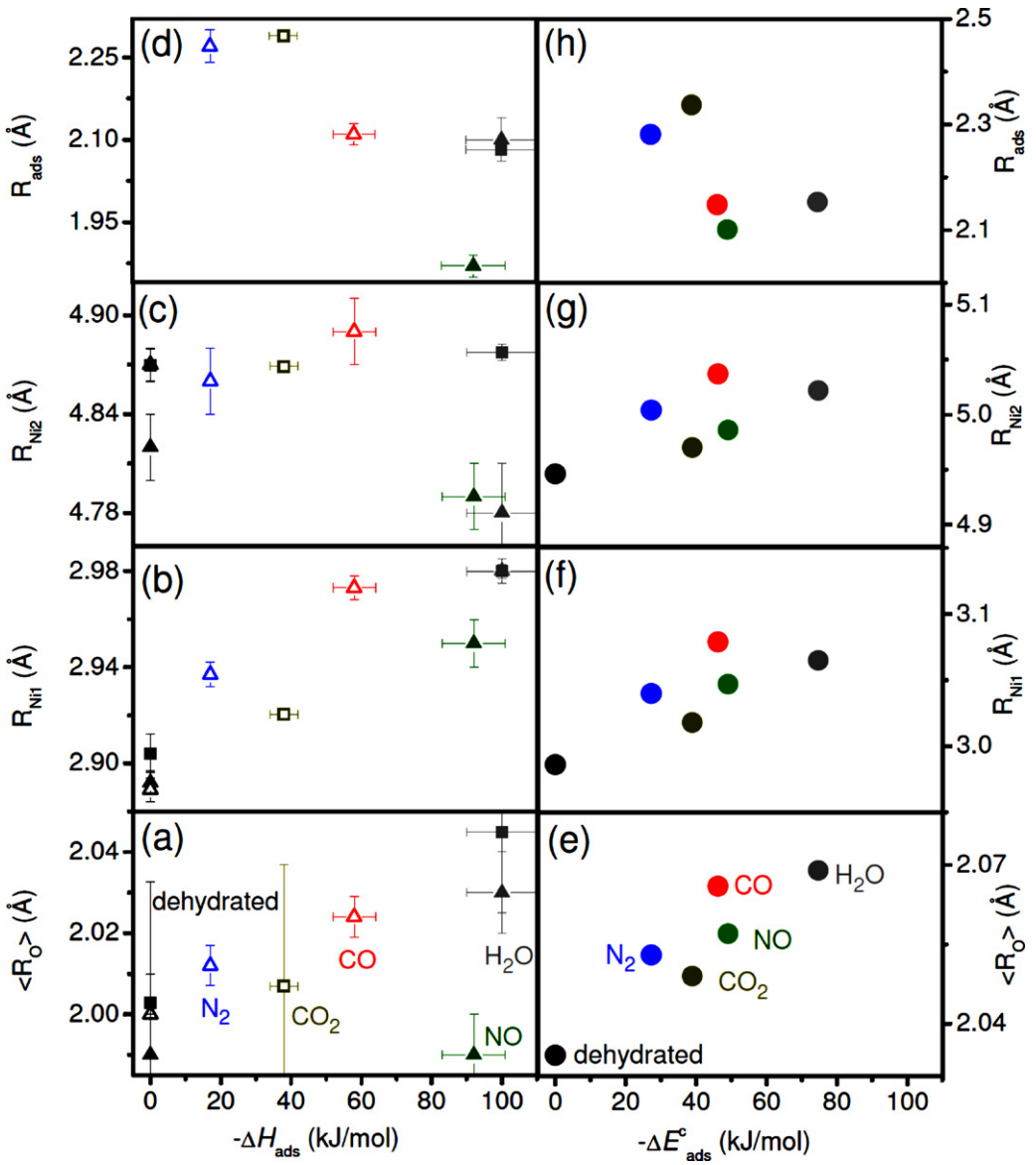

Fig. 9. Correlation of the different structural parameters upon molecular adsorption on Ni^{2+} site with the corresponding adsorption energy. Left: experimental values (XRPD circles, EXAFS triangles) and corresponding incertitudes. Full and open symbols refer data collected at 300 and 77 K, respectively. Right: theoretical values. Please note that left and right parts do not have exactly the same ordinate intervals. This reflects the systematic overestimation of the theoretical distances. Beside this fact all trends are well reproduced. Unpublished.

including the dispersion corrections (not reported for brevity), being responsible of half (or more) of the binding computed with the B3LYP-D* method. As an example, for CO the dispersion correction is $\Delta E^* = 21.3\,kJ\,mol^{-1}$ out of $46.2\,kJ\,mol^{-1}$ (i.e. 46%), while for CO_2 it is $\Delta E^* = 26.9\,kJ\,mol^{-1}$ out of $38.9\,kJ\,mol^{-1}$ (i.e. 69%). The larger dispersion contribution observed for CO_2 is ascribable to its higher polarizability. The relevance of dispersion interactions in these systems has already been reported for the homologue CPO-27-Mg material by Valenzano et al. [125].

The sum of ZPE and thermal correction to enthalpy is a small fraction of the total adsorption enthalpy for both CO and CO_2, being around 2–3 kJ mol^{-1} at 100 K and 4 kJ mol^{-1} at 298 K. For CPO-27-Mg, roughly the same values were obtained [125]. As expected, for CO the predicted adsorption enthalpy for CPO-27-Ni is larger than for the one reported for CPO-27-Mg, although it is underestimated with respect to the experimental data of -55 ± 5 and $-48\,kJ\,mol^{-1}$. If we assume this is a general result, we can estimate that the adsorption enthalpy for NO and N_2 would be -47.1 and $-25.3\,kJ\,mol^{-1}$ at 100 K and -45.1 and $-23.3\,kJ\,mol^{-1}$ at 298 K.

Summarizing, with respect to experimental evidence (Table 3), heats of adsorption of molecules adsorbed on CPO-27-Ni, computed at B3LYP-D* level of theory, are overestimated for N_2, in perfect agreement for CO_2, slightly underestimated for CO and, markedly underestimated for NO. This can be explained by considering that the DFT contribution to the binding given by B3LYP is known to be underestimated because of a poor description of charge transfer effects that take place in particular for NO and CO [180,181].

3.3.3. *Correlation among structural and energetic data*

Structural and energetic data, for the whole set of investigated molecules interacting with CPO-27-Ni have been summarized in Fig. 9. Parts (a)–(d) for the experimental values (structural from: XRPD and XAFS; and energetic from: microcalorimetry, VTIR and isosteric heat of adsorption) and parts (e)–(h) for the theoretical ones. From the reported set of data, it clearly emerges that

computed framework distances and computed adsorption distances are systematically overestimated by the theory.

Notwithstanding this fact, the trends observed in the experimental data are clearly mirrored by the theoretical data. In particular, it emerges from both experimental and theoretical data that, the larger is the adsorption energy, the larger is the perturbation induced by the adsorbed molecule to the MOF framework in terms of elongation of $\langle R_O \rangle$, R_{Ni1} and R_{Ni2} distances, see parts (a)–(c) and (e)–(g) of Fig. 9, respectively. As far as the adsorption distance is concerned, it follows an opposite trend: the larger is the $-\Delta H_{ads}$ ($-\Delta E^c{}_{ads}$), the shorter is R_{ads}, see Fig. 9(d) and Fig. 9(h), respectively.

More in detail, the following considerations can be underlined. For what concerns the EXAFS results obtained for the degassed CPO-27-Ni, it is worth noticing as $\langle R_O \rangle$, and R_{Ni2} increase by decreasing the temperature from RT (filled triangles) to 77 K (empty triangles) while R_{Ni1} does not change. An increase in the cell volume by decreasing the temperature indicates a negative thermal expansion coefficient, accordingly to what observed in other MOFs (as MOF-5) [186]. For what concerns the calculations they predict upon the adsorption an increase of all the framework distances considered and an almost linear relationship between the adsorption energy and the distance elongation. These findings have been confirmed by the experiments: as a general statement both XRD and EXAFS indicate an increase of all the framework distances upon the adsorption. However, in the experiments a larger spread of the data is observed due to the different coverages adopted in the different experiments. In fact, whereas in the calculations the coverage was fixed to Ni:molecule = 1:1, in the XRD for CO_2 and H_2O a Ni:CO_2 = 1:0.5–0.6 and Ni:H_2O = 1:5 where adopted. It is likely ascribable to the different coverage the different behavior observed for H_2O adsorption of R_{Ni2} obtained with EXAFS and XRD that indicate respectively a shortening and a lengthening of this distance. In fact, whereas the XRD data have been recorded for the highest coverage, the EXAFS measurements have been recorded at a lower Ni:H_2O ratio and then the Ni_{ads}–Ni_2 shortening is a reflection of the high interaction energy. In fact a shortening of R_{Ni2} has been also observed for NO, the second in interaction energy between them considered in this study.

Coming to the distance between the Ni atom and the adsorbed molecules (R_{ads}), in this case an opposite trend is observed in both experiments and calculations as expected: in fact this distance shortens by increasing the energetic of the interaction, the shortest distances being observed for the larger interacting molecules that is for H_2O and NO.

4. Conclusions

CPO-27-Ni MOF has been chosen as key study material to show how XRPD, EXAFS, Raman, IR, microcalorimetric data, supported by periodic DFT calculation can provide a complete picture on the structural, vibrational and energetic features of the interaction of an adsorbed molecule with the coordinatively unsaturated metal centres of desolvated MOFs frameworks. This thesis has been claimed for a large set of adsorbed molecules, namely: H_2O, NO, CO, CO_2, N_2, C_2H_4 and H_2. This multi technical approach is of general validity and can be straightforwardly extended to all MOF materials.

Our multitechnical approach is relevant in understanding and foreseeing applications to a potential practical use of MOF materials. Indeed, the understanding of the molecular adsorption on a given surface site is the first step in understanding whether the site may have a potential catalytic reactivity or not. On the other hand, measuring (and/or computing) adsorption enthalpies of different molecules allows to establish an adsorption strength scale that is relevant in determining a selective adsorption ranking useful for gas separation and selective adsorption purposes. More in detail: (i) the significant difference in the $-\Delta H_{ads}$ (and $-\Delta E^c{}_{ads}$) for the adsorption of H_2 and CO implies that CPO-27-Ni is an interesting material for the purification of a H_2/CO mixture used to feed fuel cells. (ii) The material can clearly play a role also in the CO_2 capture, even at relatively high temperatures, i.e. for *post-combustion* capture as demonstrated by the work of Dietzel et al. [124]. (iii) Finally, the ability of H_2O to progressively displace NO from the Ni^{2+} sites [126], makes CPO-27-Ni a good candidate for a controlled NO drug delivery inside the human body, similarly to the HKUST-1 MOF investigated by the group of Morris [70,187].

Acknowledgments

We are indebted to PDC Dietzel for the synthesis of high quality CPO-27-Ni MOF and to C. Prestipino for his friendly and important support during the EXAFS acquisition at ESRF BM29. This work, in particularly the grant for LV, has been supported by MOFCAT EU-project.

References

[1] G.T. Kokotailo, S.L. Lawton, W.M. Meier, Nature 272 (1978) 437.
[2] B.M. Lok, C.A. Messina, R. Lyle Patton, R.T. Gajek, T.R. Cannan, E.M. Flanigen, J. Am. Chem. Soc. 106 (1984) 6092.
[3] M.E. Davis, R.F. Lobo, Chem. Mater. 4 (1992) 756.
[4] G.A. Ozin, Adv. Mater. 4 (1992) 612.
[5] M. Shelef, Chem. Rev. 95 (1995) 209.
[6] R.A. van Santen, G.J. Kramer, Chem. Rev. 95 (1995) 637.
[7] A. Corma, Chem. Rev. 95 (1995) 559.
[8] B. Notari, Adv. Catal. 41 (1996) 253.
[9] R.E. Morris, S.J. Weigel, Chem. Soc. Rev. 26 (1997) 309.
[10] I.W.C.E. Arends, R.A. Sheldon, M. Wallau, U. Schuchardt, Angew. Chem. Int. Ed. Engl. 36 (1997) 1144.
[11] R. Krishna, B. Smit, S. Calero, Chem. Soc. Rev. 31 (2002) 185.
[12] M.E. Davis, Nature 417 (2002) 813.
[13] A. Stein, Adv. Mater. 15 (2003) 763.
[14] M. Bjorgen, F. Bonino, S. Kolboe, K.P. Lillerud, A. Zecchina, S. Bordiga, J. Am. Chem. Soc. 125 (2003) 15863.
[15] J.F. Haw, W.G. Song, D.M. Marcus, J.B. Nicholas, Acc. Chem. Res. 36 (2003) 317.
[16] A. Zecchina, S. Bordiga, J.G. Vitillo, G. Ricchiardi, C. Lamberti, G. Spoto, M. Bjorgen, K.P. Lillerud, J. Am. Chem. Soc. 127 (2005) 6361.
[17] J. Perez-Ramirez, C.H. Christensen, K. Egeblad, C.H. Christensen, J.C. Groen, Chem. Soc. Rev. 37 (2008) 2530.
[18] J.A. van Bokhoven, T.L. Lee, M. Drakopoulos, C. Lamberti, S. Thiess, J. Zegenhagen, Nat. Mater. 7 (2008) 551.
[19] G. Agostini, C. Lamberti, L. Palin, M. Milanesio, N. Danilina, B. Xu, M. Janousch, J.A. van Bokhoven, J. Am. Chem. Soc. 132 (2010) 667.
[20] R.E. Morris, X.H. Bu, Nat. Chem. 2 (2010) 353.
[21] A.K. Cheetham, G. Ferey, T. Loiseau, Angew. Chem. Int. Ed. 38 (1999) 3268.
[22] S.L. James, Chem. Soc. Rev. 32 (2003) 276.
[23] D. Bradshaw, J.B. Claridge, E.J. Cussen, T.J. Prior, M.J. Rosseinsky, Acc. Chem. Res. 38 (2005) 273.
[24] G. Ferey, Chem. Soc. Rev. 37 (2008) 191.
[25] M. O'Keeffe, Chem. Soc. Rev. 38 (2009) 1215.
[26] J.J. Perry I.V., J.A. Perman, M.J. Zaworotko, Chem. Soc. Rev. 38 (2009) 1400.
[27] H. Furukawa, N. Ko, Y.B. Go, N. Aratani, S.B. Choi, E. Choi, A.O. Yazaydin, R.Q. Snurr, M. O'Keeffe, J. Kim, O.M. Yaghi, Science 329 (2010) 424.
[28] O.K. Farha, J.T. Hupp, Acc. Chem. Res. 43 (2010) 1166.
[29] G. Seeber, G.J.T. Cooper, G.N. Newton, M.H. Rosnes, D.L. Long, B.M. Kariuki, P. Kogerler, L. Cronin, Chem. Sci. 1 (2010) 62.
[30] S. Bordiga, F. Bonino, K.P. Lillerud, C. Lamberti, Chem. Soc. Rev. 39 (2010) 4885.
[31] G. Ferey, Chem. Mater. 13 (2001) 3084.
[32] M. Eddaoudi, D.B. Moler, H.L. Li, B.L. Chen, T.M. Reineke, M. O'Keeffe, O.M. Yaghi, Acc. Chem. Res. 34 (2001) 319.
[33] J.R. Long, O.M. Yaghi, Chem. Soc. Rev. 38 (2009) 1213.
[34] D.J. Tranchemontagne, J.L. Mendoza-Cortes, M. O'Keeffe, O.M. Yaghi, Chem. Soc. Rev. 38 (2009) 1257.
[35] M. Eddaoudi, J. Kim, N. Rosi, D. Vodak, J. Wachter, M. O'Keeffe, O.M. Yaghi, Science 295 (2002) 469.
[36] J.H. Cavka, S. Jakobsen, U. Olsbye, N. Guillou, C. Lamberti, S. Bordiga, K.P. Lillerud, J. Am. Chem. Soc. 130 (2008) 13850.
[37] U. Müller, M. Schubert, F. Teich, H. Puetter, K. Schierle-Arndt, J. Pastre, J. Mater. Chem. 16 (2006) 626.
[38] A. Czaja, T. Trukhan, U. Müller, Chem. Soc. Rev. 38 (2009) 1284.
[39] M. Dinca, J.R. Long, J. Am. Chem. Soc. 127 (2005) 9376.
[40] L. Pan, D.H. Olson, L.R. Ciemnolonski, R. Heddy, J. Li, Angew. Chem. Int. Ed. 45 (2006) 616.
[41] J.-R. Li, R.J. Luppler, H.C. Zhou, Chem. Soc. Rev. 38 (2009) 1477.
[42] D. Britt, H. Furukawa, B. Wang, T.G. Glover, O.M. Yaghi, Proc. Natl. Acad. Sci. U.S.A. 106 (2009) 20637.

[43] D. Tanaka, A. Henke, K. Albrecht, M. Moeller, K. Nakagawa, S. Kitagawa, J. Groll, Nat. Chem. 2 (2010) 410.
[44] H. Sato, R. Matsuda, K. Sugimoto, M. Takata, S. Kitagawa, Nat. Mater. 9 (2010) 661.
[45] S. Shimomura, M. Higuchi, R. Matsuda, K. Yoneda, Y. Hijikata, Y. Kubota, Y. Mita, J. Kim, M. Takata, S. Kitagawa, Nat. Chem. 2 (2010) 633.
[46] R. Matsuda, T. Tsujino, H. Sato, Y. Kubota, K. Morishige, M. Takata, S. Kitagawa, Chem. Sci. 1 (2010) 315.
[47] S. Keskin, T.M. van Heest, D.S. Sholl, ChemSusChem 3 (2010) 879.
[48] G. Ferey, C. Serre, T. Devic, G. Maurin, H. Jobic, P.L. Llewellyn, G. De Weireld, A. Vimont, M. Daturi, J.S. Chang, Chem. Soc. Rev. 40 (2011) 550.
[49] K.A. Cychosz, R. Ahmad, A.J. Matzger, Chem. Sci. 1 (2010) 293.
[50] M.R. Kishan, J. Tian, P.K. Thallapally, C.A. Fernandez, S.J. Dalgarno, J.E. Warren, B.P. McGrail, J.L. Atwood, Chem. Commun. 46 (2010) 538.
[51] Y.S. Li, F.Y. Liang, H. Bux, A. Feldhoff, W.S. Yang, J. Caro, Angew. Chem. Int. Ed. 49 (2010) 548.
[52] J. An, S.J. Geib, N.L. Rosi, J. Am. Chem. Soc. 132 (2010) 38.
[53] M. Kondo, T. Yoshitomi, K. Seki, H. Matsuzaka, S. Kitagawa, Angew. Chem. Int. Ed. Engl. 36 (1997) 1725.
[54] A.R. Millward, O.M. Yaghi, J. Am. Chem. Soc. 127 (2005) 17998.
[55] D.F. Sun, S.Q. Ma, Y.X. Ke, D.J. Collins, H.C. Zhou, J. Am. Chem. Soc. 128 (2006) 3896.
[56] Y.W. Li, R.T. Yang, J. Am. Chem. Soc. 128 (2006) 726.
[57] M. Dinca, A. Dailly, Y. Liu, C.M. Brown, D.A. Neumann, J.R. Long, J. Am. Chem. Soc. 128 (2006) 16876.
[58] P.M. Forster, J. Eckert, B.D. Heiken, J.B. Parise, J.W. Yoon, S.H. Jhung, J.S. Chang, A.K. Cheetham, J. Am. Chem. Soc. 128 (2006) 16846.
[59] P.D.C. Dietzel, R.E. Johnsen, H. Fjellvag, S. Bordiga, E. Groppo, S. Chavan, R. Blom, Chem. Commun. (2008) 5125.
[60] J.G. Vitillo, L. Regli, S. Chavan, G. Ricchiardi, G. Spoto, P.D.C. Dietzel, S. Bordiga, A. Zecchina, J. Am. Chem. Soc. 130 (2008) 8386.
[61] S.Q. Ma, D.F. Sun, J.M. Simmons, C.D. Collier, D.Q. Yuan, H.C. Zhou, J. Am. Chem. Soc. 130 (2008) 1012.
[62] A.P. Nelson, O.K. Farha, K.L. Mulfort, J.T. Hupp, J. Am. Chem. Soc. 131 (2009) 458.
[63] L.J. Murray, M. Dinca, J.R. Long, Chem. Soc. Rev. 38 (2009) 1294.
[64] H. Wu, W. Zhou, T. Yildirim, J. Am. Chem. Soc. 131 (2009) 4995.
[65] S.S. Han, J.L. Mendoza-Cortes, W.A. Goddard, Chem. Soc. Rev. 38 (2009) 1460.
[66] Y.H. Hu, L. Zhang, Adv. Mater. 22 (2010) E117.
[67] D.M. D'Alessandro, B. Smit, J.R. Long, Angew. Chem. Int. Ed. 49 (2010) 6058.
[68] K. Sumida, S. Horike, S.S. Kaye, Z.R. Herm, W.L. Queen, C.M. Brown, F. Grandjean, G.J. Long, A. Dailly, J.R. Long, Chem. Sci. 1 (2010) 184.
[69] K. Sumida, C.M. Brown, Z.R. Herm, S. Chavan, S. Bordiga, J.R. Long, Chem. Commun. 47 (2011) 1157.
[70] B. Xiao, P.S. Wheatley, X.B. Zhao, A.J. Fletcher, S. Fox, A.G. Rossi, I.L. Megson, S. Bordiga, L. Regli, K.M. Thomas, R.E. Morris, J. Am. Chem. Soc. 129 (2007) 1203.
[71] P. Horcajada, T. Chalati, C. Serre, B. Gillet, C. Sebrie, T. Baati, J.F. Eubank, D. Heurtaux, P. Clayette, C. Kreuz, J.S. Chang, Y.K. Hwang, V. Marsaud, P.N. Bories, L. Cynober, S. Gil, G. Ferey, P. Couvreur, R. Gref, Nat. Mater. 9 (2010) 172.
[72] J.C.G. Bunzli, C. Piguet, Chem. Rev. 102 (2002) 1897.
[73] C. Serre, F. Millange, C. Thouvenot, N. Gardant, F. Pelle, G. Ferey, J. Mater. Chem. 14 (2004) 1540.
[74] D. Imbert, S. Comby, A.S. Chauvin, J.C.G. Bunzli, Chem. Commun. (2005) 1432.
[75] S. Bordiga, C. Lamberti, G. Ricchiardi, L. Regli, F. Bonino, A. Damin, K.P. Lillerud, M. Bjorgen, A. Zecchina, Chem. Commun. (2004) 2300.
[76] M.D. Allendorf, C.A. Bauer, R.K. Bhakta, R.J.T. Houk, Chem. Soc. Rev. 38 (2009) 1330.
[77] D. Maspoch, D. Ruiz-Molina, K. Wurst, N. Domingo, M. Cavallini, F. Biscarini, J. Tejada, C. Rovira, J. Veciana, Nat. Mater. 2 (2003) 190.
[78] D. Maspoch, N. Domingo, D.R. Molina, K. Wurst, J.M. Hernandez, G. Vaughan, C. Rovira, F. Lloret, J. Tejada, J. Veciana, Chem. Commun. (2005) 5035.
[79] M. Kurmoo, Chem. Soc. Rev. 38 (2009) 1353.
[80] G. Ferey, F. Millange, M. Morcrette, C. Serre, M.L. Doublet, J.M. Greneche, J.M. Tarascon, Angew. Chem. Int. Ed. 46 (2007) 3259.
[81] C.G. Silva, A. Corma, H. Garcia, J. Mater. Chem. 20 (2010) 3141.
[82] S.L. Qiu, G.S. Zhu, Coord. Chem. Rev. 253 (2009) 2891.
[83] Z.G. Xie, L.Q. Ma, K.E. deKrafft, A. Jin, W.B. Lin, J. Am. Chem. Soc. 132 (2010) 922.
[84] P.M. Forster, A.K. Cheetham, Top. Catal. 24 (2003) 79.
[85] B. Kesanli, W.B. Lin, Coord. Chem. Rev. 246 (2003) 305.
[86] K. Schlichte, T. Kratzke, S. Kaskel, Micropor. Mesopor. Mater. 73 (2004) 81.
[87] C.D. Wu, A. Hu, L. Zhang, W.B. Lin, J. Am. Chem. Soc. 127 (2005) 8940.
[88] S. Hermes, M.-K. Schröter, R. Schmid, L. Khodeir, M. Muhler, A. Tissler, R.W. Fischer, R.A. Fischer, Angew. Chem. Int. Ed. 44 (2005) 6237.
[89] D.N. Dybtsev, A.L. Nuzhdin, H. Chun, K.P. Bryliakov, E.P. Talsi, V.P. Fedin, K. Kim, Angew. Chem. Int. Ed. 45 (2006) 916.
[90] F.X. Llabrés i Xamena, A. Abad, A. Corma, H. Garcia, J. Catal. 250 (2007) 294.
[91] B. Xiao, H.W. Hou, Y.T. Fan, J. Organomet. Chem. 692 (2007) 2014.
[92] Y. Goto, H. Sato, S. Shinkai, K. Sada, J. Am. Chem. Soc. 130 (2008) 14354.
[93] S. Proch, J. Herrmannsdorfer, R. Kempe, C. Kern, A. Jess, L. Seyfarth, J. Senker, Chem. Eur. J. 14 (2008) 8204.
[94] S. Horike, M. Dinca, K. Tamaki, J.R. Long, J. Am. Chem. Soc. 130 (2008) 5854.
[95] M. Savonnet, S. Aguado, U. Ravon, D. Bazer-Bachi, V. Lecocq, N. Bats, C. Pinel, D. Farrusseng, Green Chem. 11 (2009) 1729.
[96] S. Das, H. Kim, K. Kim, J. Am. Chem. Soc. 131 (2009) 3814.
[97] J. Gascon, U. Aktay, M.D. Hernandez-Alonso, G.P.M. van Klink, F. Kapteijn, J. Catal. 261 (2009) 75.
[98] D.M. Jiang, A. Urakawa, M. Yulikov, T. Mallat, G. Jeschke, A. Baiker, Chem. Eur. J. 15 (2009) 12255.
[99] J. Lee, O.K. Farha, J. Roberts, K.A. Scheidt, S.T. Nguyen, J.T. Hupp, Chem. Soc. Rev. 38 (2009) 1450.
[100] A.M. Shultz, O.K. Farha, J.T. Hupp, S.T. Nguyen, J. Am. Chem. Soc. 131 (2009) 4204.
[101] L. Ma, C. Abney, W. Lin, Chem. Soc. Rev. 38 (2009) 1248.
[102] A. Corma, H. Garcıa, F.X. Llabres i Xamena, Chem. Rev. 110 (2010) 4606.
[103] J. Juan-Alcaniz, E.V. Ramos-Fernandez, U. Lafont, J. Gascon, F. Kapteijn, J. Catal. 269 (2010) 229.
[104] D.M. Jiang, T. Mallat, D.M. Meier, A. Urakawa, A. Baiker, J. Catal. 270 (2010) 26.
[105] I. Luz, F. Xamena, A. Corma, J. Catal. 276 (2010) 134.
[106] S.X. Gao, N. Zhao, M.H. Shu, S.N. Che, Appl. Catal. A-Gen. 388 (2010) 196.
[107] F.J. Song, C. Wang, J.M. Falkowski, L.Q. Ma, W.B. Lin, J. Am. Chem. Soc. 132 (2010) 15390.
[108] A. Dhakshinamoorthy, M. Alvaro, H. Garcia, Adv. Synth. Catal. 352 (2010) 3022.
[109] D.B. Dang, P.Y. Wu, C. He, Z. Xie, C.Y. Duan, J. Am. Chem. Soc. 132 (2010) 14321.
[110] Y. Liu, W.M. Xuan, Y. Cui, Adv. Mater. 22 (2010) 4112.
[111] Y.Q. Li, P. Song, J. Zheng, X.G. Li, Chem. Eur. J. 16 (2010) 10887.
[112] H.L. Liu, Y.L. Liu, Y.W. Li, Z.Y. Tang, H.F. Jiang, J. Phys. Chem. C 114 (2010) 13362.
[113] R. Makiura, S. Motoyama, Y. Umemura, H. Yamanaka, O. Sakata, H. Kitagawa, Nat. Mater. 9 (2010) 565.
[114] K.P. Lillerud, U. Olsbye, M. Tilset, Top. Catal. 53 (2010) 859.
[115] G.A.E. Oxford, D. Dubbeldam, L.J. Broadbelt, R.Q. Snurr, J. Mol. Catal. A-Chem. 334 (2011) 89.
[116] F. Vermoortele, R. Ameloot, A. Vimont, C. Serre, D. De Vos, Chem. Commun. 47 (2011) 1521.
[117] M. Ranocchiari, J.A. van Bokhoven, Phys. Chem. Chem. Phys. 13 (2011) 6388.
[118] C.G. Silva, I. Luz, F.X. Llabres i Xamena, A. Corma, H. Garcia, Chem. Eur. J. 16 (2010) 11133.
[119] P.D.C. Dietzel, B. Panella, M. Hirscher, R. Blom, H. Fjellvag, Chem. Commun. (2006) 959.
[120] N.L. Rosi, J. Kim, M. Eddaoudi, B.L. Chen, M. O'Keeffe, O.M. Yaghi, J. Am. Chem. Soc. 127 (2005) 1504.
[121] P.D.C. Dietzel, Y. Morita, R. Blom, H. Fjellvag, Angew. Chem. Int. Ed. 44 (2005) 6354.
[122] P.D.C. Dietzel, R.E. Johnsen, R. Blom, H. Fjellvåg, Chem. Eur. J. 14 (2008) 2389.
[123] S.R. Caskey, A.G. Wong-Foy, A.J. Matzger, J. Am. Chem. Soc. 130 (2008) 10870.
[124] P.D.C. Dietzel, V. Besikiotis, R. Blom, J. Mater. Chem. 19 (2009) 7362.
[125] L. Valenzano, B. Civalleri, S. Chavan, G.T. Palomino, C.O. Arean, S. Bordiga, J. Phys. Chem. C 114 (2010) 11185.
[126] F. Bonino, S. Chavan, J.G. Vitillo, E. Groppo, G. Agostini, C. Lamberti, P.D.C. Dietzel, C. Prestipino, S. Bordiga, Chem. Mater. 20 (2008) 4957.
[127] S. Chavan, J.G. Vitillo, E. Groppo, F. Bonino, C. Lamberti, P.D.C. Dietzel, S. Bordiga, J. Phys. Chem. C 113 (2009) 3292.
[128] S. Chavan, F. Bonino, J.G. Vitillo, E. Groppo, C. Lamberti, P.D.C. Dietzel, A. Zecchina, S. Bordiga, Phys. Chem. Chem. Phys. 11 (2009) 9811.
[129] R. Dovesi, R. Orlando, B. Civalleri, C. Roetti, V.R. Saunders, C.M. Zicovich-Wilson, Z. Kristallogr. 220 (2005) 571.
[130] R. Dovesi, V.R. Saunders, R. Roetti, R. Orlando, C.M. Zicovich-Wilson, F. Pascale, B. Civalleri, K. Doll, N.M. Harrison, I.J. Bush, P. D'Arco, M. Llunell, CRYSTAL09, University of Torino, 2009.
[131] L. Valenzano, B. Civalleri, S. Bordiga, M.H. Nilsen, S. Jakobsen, K.-P. Lillerud, C. Lamberti, Chem. Mater. 23 (2011) 1700.
[132] V. Bolis, S. Bordiga, C. Lamberti, A. Zecchina, A. Carati, F. Rivetti, G. Spano, G. Petrini, Langmuir 15 (1999) 5753.
[133] V. Bolis, S. Maggiorini, L. Meda, F. D'Acapito, G.T. Palomino, S. Bordiga, C. Lamberti, J. Chem. Phys. 113 (2000) 9248.
[134] S. Bordiga, I. Roggero, P. Ugliengo, A. Zecchina, V. Bolis, G. Artioli, R. Buzzoni, G.L. Marra, F. Rivetti, G. Spanò, C. Lamberti, J. Chem. Soc., Dalton Trans. (2000) 3921.
[135] S. Bordiga, A. Damin, F. Bonino, A. Zecchina, G. Spanò, F. Rivetti, V. Bolis, C. Lamberti, J. Phys. Chem. B 106 (2002) 9892.
[136] V. Bolis, A. Barbaglia, S. Bordiga, C. Lamberti, A. Zecchina, J. Phys. Chem. B 108 (2004) 9970.
[137] J. Estephane, E. Groppo, J.G. Vitillo, A. Damin, C. Lamberti, S. Bordiga, A. Zecchina, Phys. Chem. Chem. Phys. 11 (2009) 2218.
[138] G. Spoto, E. Gribov, S. Bordiga, C. Lamberti, G. Ricchiardi, D. Scarano, A. Zecchina, Chem. Commun. (2004) 2768.
[139] G. Spoto, E.N. Gribov, G. Ricchiardi, A. Damin, D. Scarano, S. Bordiga, C. Lamberti, A. Zecchina, Prog. Surf. Sci. 76 (2004) 71.
[140] C. Lamberti, E. Groppo, G. Spoto, S. Bordiga, A. Zecchina, Adv. Catal. 51 (2007) 1.
[141] C. Lamberti, A. Zecchina, E. Groppo, S. Bordiga, Chem. Soc. Rev. 39 (2010) 4951.
[142] A. Filipponi, M. Borowski, D.T. Bowron, S. Ansell, A. Di Cicco, S. De Panfilis, J.P. Itie, Rev. Sci. Instrum. 71 (2000) 2422.
[143] C. Lamberti, S. Bordiga, F. Bonino, C. Prestipino, G. Berlier, L. Capello, F. D'Acapito, F.X.L.I. Xamena, A. Zecchina, Phys. Chem. Chem. Phys. 5 (2003) 4502.
[144] C. Lamberti, C. Prestipino, S. Bordiga, G. Berlier, G. Spoto, A. Zecchina, A. Laloni, F. La Manna, F. D'Anca, R. Felici, F. D'Acapito, P. Roy, Nucl. Instrum. Methods B 200 (2003) 196.

[145] K.V. Klementev, Nucl. Instrum. Methods Phys. Res. A 448 (2000) 299.
[146] B. Ravel, M. Newville, J. Synchrot. Radiat. 12 (2005) 537.
[147] S.I. Zabinsky, J.J. Rehr, A. Ankudinov, R.C. Albers, M.J. Eller, Phys. Rev. B 52 (1995) 2995.
[148] C. Lamberti, E. Groppo, C. Prestipino, S. Casassa, A.M. Ferrari, C. Pisani, C. Giovanardi, P. Luches, S. Valeri, F. Boscherini, Phys. Rev. Lett 91 (2003), Art. n. 046101.
[149] E. Groppo, C. Prestipino, C. Lamberti, P. Luches, C. Giovanardi, F. Boscherini, J. Phys. Chem. B 107 (2003) 4597.
[150] A.D. Becke, J. Chem. Phys. 98 (1993) 5648.
[151] C. Lee, W. Yang, R.G. Parr, Phys. Rev. B 37 (1988) 785.
[152] B. Miehlich, A. Savin, H. Stoll, H. Preuss, Chem. Phys. Lett. 157 (1989) 200.
[153] S. Grimme, J. Comput. Chem. 27 (2006) 1787.
[154] B. Civalleri, C.M. Zicovich-Wilson, L. Valenzano, P. Ugliengo, Crystengcomm 10 (2008) 405.
[155] S.F. Boys, F. Bernardi, Mol. Phys. 19 (1970) 553.
[156] F. Pascale, C.M. Zicovich-Wilson, F. López Gejo, B. Civalleri, R. Orlando, R. Dovesi, J. Comput. Chem. 25 (2004) 888.
[157] L. Valenzano, B. Civalleri, K. Sillar, J. Sauer, J. Phys. Chem. C, submitted for publication.
[158] G. Ferey, C. Serre, Chem. Soc. Rev. 38 (2009) 1280.
[159] H. Kitagawa, Y. Nagao, M. Fujishima, R. Ikeda, S. Kanda, Inorg. Chem. Commun. 6 (2003) 346.
[160] H. Dathe, E. Peringer, V. Roberts, A. Jentys, J.A. Lercher, C R Chim. 8 (2005) 753.
[161] H. Dathe, A. Jentys, J.A. Lercher, Phys. Chem. Chem. Phys. 7 (2005) 1283.
[162] H. Dathe, A. Jentys, J.A. Lercher, Stud. Surf. Sci. Catal. 158 (2005) 995.
[163] S. Surble, F. Millange, C. Serre, G. Ferey, R.I. Walton, Chem. Commun. (2006) 1518.
[164] K.C. Szeto, K.P. Lillerud, M. Tilset, M. Bjorgen, C. Prestipino, A. Zecchina, C. Lamberti, S. Bordiga, J. Phys. Chem. B 110 (2006) 21509.
[165] K.C. Szeto, C. Prestipino, C. Lamberti, A. Zecchina, S. Bordiga, M. Bjorgen, M. Tilset, K.P. Lillerud, Chem. Mater. 19 (2007) 211.
[166] C. Prestipino, L. Regli, J.G. Vitillo, F. Bonino, A. Damin, C. Lamberti, A. Zecchina, P.L. Solari, K.O. Kongshaug, S. Bordiga, Chem. Mater. 18 (2006) 1337.
[167] J. Hafizovic, M. Bjorgen, U. Olsbye, P.D.C. Dietzel, S. Bordiga, C. Prestipino, C. Lamberti, K.P. Lillerud, J. Am. Chem. Soc. 129 (2007) 3612.
[168] M. Seredyuk, A.B. Gaspar, V. Ksenofontov, M. Verdaguer, F. Villain, P. Gutlich, Inorg. Chem. 48 (2009) 6130.
[169] G. de Combarieu, S. Hamelet, F. Millange, M. Morcrette, J.M. Tarascon, G. Ferey, R.I. Walton, Electrochem. Commun. 11 (2009) 1881.
[170] N. Masciocchi, S. Galli, V. Colombo, A. Maspero, G. Palmisano, B. Seyyedi, C. Lamberti, S. Bordiga, J. Am. Chem. Soc. 132 (2010) 7902.
[171] S. Gross, M. Bauer, Adv. Funct. Mater. 20 (2010) 4026.
[172] A. Filipponi, A. Dicicco, R. Zanoni, M. Bellatreccia, V. Sessa, C. Dossi, R. Psaro, Chem. Phys. Lett. 184 (1991) 485.
[173] R. Crusemann, F. Bokman, V. Fritzsche, H. Bertagnolli, Chem. Phys. 194 (1995) 81.
[174] C. Lamberti, G.T. Palomino, S. Bordiga, G. Berlier, F. D'Acapito, A. Zecchina, Angew. Chem. Int. Ed. 39 (2000) 2138.
[175] D. Gianolio, E. Groppo, J.G. Vitillo, A. Damin, S. Bordiga, A. Zecchina, C. Lamberti, Chem. Commun. 46 (2010) 976.
[176] S. Chavan, J.G. Vitillo, M.J. Uddin, F. Bonino, C. Lamberti, E. Groppo, K.P. Lillerud, S. Bordiga, Chem. Mater. 22 (2010) 4602.
[177] R.J. Lobo-Lapidus, B.C. Gates, Langmuir 26 (2010) 16368.
[178] H. Kuhlenbeck, G. Odorfer, R. Jaeger, G. Illing, M. Menges, T. Mull, H.J. Freund, M. Pohlchen, V. Staemmler, S. Witzel, C. Scharfschwerdt, K. Wennemann, T. Liedtke, M. Neumann, Phys. Rev. B 43 (1991) 1969.
[179] R. Lindsay, P. Baumgartel, R. Terborg, O. Schaff, A.M. Bradshaw, D.P. Woodruff, Surf. Sci. 425 (1999) L401.
[180] M. Chiesa, M.C. Paganini, E. Giamello, C. Di Valentin, G. Pacchioni, J. Mol. Catal. A-Chem. 204 (2003) 779.
[181] G. Pacchioni, C. Di Valentin, D. Dominguez-Ariza, F. Illas, T. Bredow, T. Kluner, V. Staemmler, J. Phys. Condens. Matter 16 (2004) S2497.
[182] P.D.C. Dietzel, R. Blom, H. Fjellvag, Eur. J. Inorg. Chem. (2008) 3624.
[183] R. Wysokiński, B. Morzyk-Ociepa, T. Glowiak, D. Michalska, J. Mol. Struct. 606 (2002) 241.
[184] J.G. Vitillo, M. Savonnet, G. Ricchiardi, S. Bordiga, ChemSusChem 4 (2011), doi:10.1002/cssc.201000458, in press.
[185] F. Geobaldo, C. Lamberti, G. Ricchiardi, S. Bordiga, A. Zecchina, G.T. Palomino, C.O. Arean, J. Phys. Chem. 99 (1995) 11167.
[186] N. Lock, Y. Wu, M. Christensen, L.J. Cameron, V.K. Peterson, A.J. Bridgeman, C.J. Kepert, B.B. Iversen, J. Phys. Chem. C 114 (2010) 16181.
[187] S. Bordiga, L. Regli, F. Bonino, E. Groppo, C. Lamberti, B. Xiao, P.S. Wheatley, R.E. Morris, A. Zecchina, Phys. Chem. Chem. Phys. 9 (2007) 2676.